

NASA TECHNICAL NOTE



NASA TN D-3303

e. 1

NASA TN D-3303

LOAN COPY, RETURN TO
SERIALS (MAIL-9)
LANGLEY RESEARCH CENTER

0130027



TECH LIBRARY KAFB, NM

A THEORETICAL STUDY OF THE EFFECT
ON EXPANSION-TUBE PERFORMANCE
OF AREA CHANGES AT PRIMARY
AND SECONDARY DIAPHRAGM STATIONS

by *Linwood B. Callis, Jr.*

Langley Research Center

Langley Station, Hampton, Va.



A THEORETICAL STUDY OF THE EFFECT ON EXPANSION-TUBE
PERFORMANCE OF AREA CHANGES AT PRIMARY AND
SECONDARY DIAPHRAGM STATIONS

By Linwood B. Callis, Jr.

Langley Research Center
Langley Station, Hampton, Va.

NATIONAL AERONAUTICS AND SPACE ADMINISTRATION

For sale by the Clearinghouse for Federal Scientific and Technical Information
Springfield, Virginia 22151 - Price \$1.05

A THEORETICAL STUDY OF THE EFFECT ON EXPANSION-TUBE
PERFORMANCE OF AREA CHANGES AT PRIMARY AND
SECONDARY DIAPHRAGM STATIONS

By Linwood B. Callis, Jr.
Langley Research Center

SUMMARY

An investigation is made to determine the effect on expansion-tube performance and operating parameters of the insertion of either a nozzle or an area discontinuity in the basic expansion-tube configuration.

The present analysis is carried out with the area change located at either the primary or the secondary diaphragm. During all phases of the facility operating cycle, the assumption of a calorically perfect gas is made, thus, analytic solutions are allowed for parameters under scrutiny and trends which may be of interest are more clearly established.

From the included analysis, a determination of the performance and operating parameters of the device is made. Although certain benefits may be derived from the insertion of area changes at the locations described, other considerations make such a placement undesirable.

The advantages as well as disadvantages of the configurations considered are presented and discussed briefly.

INTRODUCTION

Trimpi (ref. 1) presented a theoretical analysis of the basic expansion tube, delineating the projected advantages and disadvantages of this device. Of the anticipated drawbacks, two prompted the analysis contained in the present paper: viscous effects encountered in the acceleration chamber and diaphragm opening problems.

The first of these problems arises as a result of the long flow lengths at low operating pressures encountered in the acceleration chamber. As a result of this combination of circumstances, the boundary-layer thickness may be found to be a significant fraction of the tube diameter, if this diameter is kept moderately small (4 to 8 inches (10 to 20 cm)). This situation may lead to boundary-layer closure at the center line, eliminating any core of potential flow, or to large flow gradients resulting from viscous attenuating

mechanisms. It is, therefore, necessary to find some means to circumvent these effects. The most obvious solution to the viscous problem, other than using tubes of large diameter, is to maintain operating pressures and flow lengths not conducive to severe boundary-layer growth. This approach, however, is not practical since, for reasonable test times, the expansion tube requires rather long flow lengths. In addition, restricting the range of operating pressures negates one of the major advantages of the facility – that is, the ability to duplicate flight environments over a wide range of velocities and ambient conditions.

It is with such considerations in mind that the analysis in the following sections is undertaken. The attitude taken is that at some point in the tube, either a nozzle or area discontinuity is present which allows the flow to expand into a tube of larger section. This area change is located at either the primary (configurations I and II) or secondary diaphragm (configuration III). In either case, the acceleration chamber has the benefit of an area enlargement, thus, ameliorating the viscous problem. At the same time, the diaphragm problem is somewhat diminished in that the use of a nozzle allows smaller upstream cross sections for a given test-section size. Thus, at least the primary and possibly the secondary diaphragm diameter is reduced depending on the configuration chosen. The diaphragms being smaller open more quickly and produce more nearly ideal wave systems and allow the facility to operate with greater efficiency.

In review, the nozzle, or area discontinuity concept, is the most direct approach to the easement of the viscous and diaphragm problems. However, along with the benefits of the nozzle configurations, certain disadvantages must also be accepted: namely, in a supersonic flow (which is presupposed behind all traveling shocks) the steady expansion is not as effective a converter of thermal to kinetic energy as in a nonsteady expansion (ref. 1) and, further, as nonsteady shock waves and/or interfaces pass through the nozzles, unsteady adjusting wave systems are necessarily generated which must be reckoned with. Such problems and their solutions are investigated and discussed.

The present analysis and that of reference 2, are complementary and together form a rather complete analysis of this type of modification to the expansion tube. From this basis, the decision as to which configuration is most feasible can be made and confirmed.

SYMBOLS

A	cross-sectional area
\bar{A}	area ratio, A_e/A_i
a	sound speed
l_d	length of driver chamber

l_n	length of nozzle
l_{s_1}	length of intermediate chamber
l_{s_2}	length of acceleration chamber
l_x	length of unusable slug test gas in region 2 for configuration III
M	Mach number
M_{es}	adjusting shock Mach number
M_{s_1}	primary shock Mach number
m_x	mass of unusable test gas for configuration III
m_5	mass of usable test gas in region 5 for configuration III
p	pressure
T	temperature
t	time
u	velocity
u_{es}	adjusting shock velocity
x	axial distance measured from primary diaphragm, except where noted
β	parameter defined by equation (45)
γ	ratio of specific heats of test gas, 1.4
$\bar{\gamma}$	ratio of specific heats of driver and acceleration chamber gas, 1.67
Δ	time interval required for wave type to pass through conical nozzle
ζ	parameter defined by equation (A4)
ξ	parameter defined by equation (39)
ρ	mass density
Φ	ratio of driver pressures, $p_{4,\bar{A}}/p_{4,\bar{A}} = 1.0$
ψ	mass ratio, m_x/m_5

Subscripts:

\bar{A}	facility with area change
b,c	general subscripts
e	steady-state conditions at nozzle exit
f	flow particle
i	steady-state conditions at nozzle inlet
m	zero length nozzle
o	constant area expansion tube
I	configuration I
II	configuration II
III	configuration III
1	initial conditions in intermediate chamber
2	conditions behind shock in intermediate chamber
3	conditions of expanded driver gas
3e	conditions behind adjusting shock
4	hot driver conditions
5	test conditions
10	initial conditions in acceleration chamber
20	conditions behind shock in acceleration chamber
+	$u + a$ characteristic
-	$u - a$ characteristic

PERFECT GAS ANALYSIS

In this analysis, all gases are assumed to be calorically perfect, since this assumption permits solutions for most of the desired parameters in closed form, which greatly facilitates the analysis yet preserves trends of interest.

Investigated in the present paper are three modifications of the basic expansion tube discussed in reference 1. These modifications are referred to as configurations I, II, and III. (See fig. 1.) Configuration I (figs. 1(a) and 2(a)) consists of the basic expansion tube with a divergent nozzle located immediately downstream of the primary diaphragm. The inlet and exit areas of the nozzle are denoted by A_i and A_e , respectively, resulting in an area ratio $\bar{A} = A_e/A_i$. The nozzle length is denoted by l_n .

Configuration I is operated as an "ideally expanded" nozzle in that the pressure and velocity of the driver gas at the nozzle exit (conditions e , fig. 1(a)) match identically those in the shock initiated flow (region 2). Thus, no waves are necessary to adjust the nozzle and shock flow to a common interface condition. Pressure ratios are taken to be such that a value of $M_i = 1$ is insured.

Configuration II is physically identical to configuration I, the difference being in the mode of operation. Configuration II is operated in the over-expanded mode which is to say $p_e < p_2$, $u_e > u_2$. Hence, an upstream-facing shock wave is required in order to bring conditions e to state $3e$, which is identical in u and p to state 2. (See fig. 1(b).) Forward-facing adjusting waves in this system are not permitted.

For configuration III (figs. 1(c) and 2(b)) the nozzle is located immediately downstream of the secondary diaphragm. This location results in the primary as well as the secondary diaphragms being reduced in size and the acceleration chamber being increased in diameter. The anticipated wave schematic for this configuration is shown in figure 1(c), which, along with figures 1(a) and 1(b), may be compared with the wave schematic of the basic expansion tube (fig. 3). Some experimental and theoretical work on this configuration has been done at Arnold Engineering Development Center.

Driver Requirements for Configuration I

One means of analyzing the present configurations is by comparing their operating parameters to those of the basic expansion tube for identical test states. Before beginning, however, the following relationships which are basic to steady and unsteady flows and used repeatedly are presented along with their regions of applicability:

$$a + \frac{\gamma - 1}{2}u = \text{Constant} \quad \begin{array}{l} \text{(Riemann, invariant for unsteady} \\ \text{isentropic constant area flow)} \end{array} \quad (1a)$$

$$a^2 + \frac{\gamma - 1}{2}u^2 = \text{Constant} \quad \text{(steady homenthalpic flow)} \quad (1b)$$

$$\frac{p_b}{p_c} = \left(\frac{a_b}{a_c}\right)^{\frac{2\gamma}{\gamma-1}} \quad \text{(isentropic)} \quad (2a)$$

$$\frac{\rho_b}{\rho_c} = \left(\frac{a_b}{a_c}\right)^{\frac{2}{\gamma-1}} \quad (\text{isentropic}) \quad (2b)$$

where the subscripts b and c refer to any two states along an isentrope.

Consider now the driver pressure required for the basic expansion tube for a given test-section Mach number M_5 . The required relation is

$$\left(\frac{p_4}{p_5}\right)_O = \left(\frac{p_4}{p_2}\right)\left(\frac{p_2}{p_5}\right) = \frac{\left(\frac{1 + \frac{\gamma-1}{2}M_5^2}{1 + \sqrt{\frac{\gamma-1}{2\gamma}}}\right)^{\frac{2\gamma}{\gamma-1}}}{\left[1 - \frac{\bar{\gamma}-1}{2} \frac{1}{(a_4/a_5)_O} \sqrt{\frac{2}{\gamma(\gamma-1)}} \left(\frac{1 + \frac{\gamma-1}{2}M_5^2}{1 + \sqrt{\frac{\gamma-1}{2\gamma}}}\right)^{\frac{2\bar{\gamma}}{\bar{\gamma}-1}}\right]} \quad (3)$$

which is equivalent to equation (36) of reference 2 for $\bar{A} = 1$ and $M_f = M_5$. In equation (3), the strong shock limit for M_2 ,

$$M_2 = \sqrt{\frac{2}{\gamma(\gamma-1)}} \quad (4)$$

has been used. Henceforth, it is assumed that all shock waves appearing in this analysis, with the exception of the adjusting shock in configuration II, are strong shocks. Equation (3) is shown plotted in figure 4 for $(a_4/a_5)_O = 5, 10,$ and 20 and for $\bar{\gamma} = 1.67$ for a helium driver.

For configuration I, the same parameter p_4/p_5 may be expressed in terms of ratios as follows:

$$\left(\frac{p_4}{p_5}\right)_I = \left(\frac{p_4}{p_i}\right)\left(\frac{p_i}{p_e}\right)\left(\frac{p_e}{p_2}\right)\left(\frac{p_2}{p_5}\right) \quad (5)$$

These ratios (eq. (5)) may be evaluated by assuming that conditions at nozzle inlet are sonic and by using equations (1a), (1b), and (2a) with the interface relation $p_2 = p_e$. When these values are substituted into equation (5), the result is

$$\left(\frac{p_4}{p_5}\right)_I = \left[\frac{\bar{\gamma} + 1}{2} \left(1 + \frac{\bar{\gamma} - 1}{2} M_e^2 \right) \right]^{\frac{\bar{\gamma}}{\bar{\gamma} - 1}} \left(\frac{1 + \frac{\gamma - 1}{2} M_5}{1 + \sqrt{\frac{\gamma - 1}{2\gamma}}} \right)^{\frac{2\gamma}{\gamma - 1}} \quad (6)$$

Implicit in equation (6) is the assumption that waves generated by the starting process of the nozzle are negligible. This assumption is discussed in a later section.

At this point, having determined p_4 so that $p_2 = p_e$, the sound speed a_4 necessary to insure that $u_e = u_2$ must be determined. Let

$$u_2 = u_e = M_e a_e \quad (7)$$

where

$$a_e = a_4 \frac{a_e}{a_4} = \frac{u_2}{M_e} \quad (8)$$

with

$$u_2 = \frac{a_5 \left(1 + \frac{\gamma - 1}{2} M_5 \right)}{\frac{1}{M_2} + \frac{\gamma - 1}{2}} \quad (9)$$

as determined from equation (1a). Substituting equation (9) and a_e/a_4 , determined from equations (1a) and (1b), into equation (8) and simplifying gives the required condition for $(a_4/a_5)_I$ as

$$\left(\frac{a_4}{a_5}\right)_I = \left[\frac{\bar{\gamma} + 1}{2} \left(1 + \frac{\bar{\gamma} - 1}{2} M_e^2 \right) \right]^{1/2} \frac{1}{M_e} \sqrt{\frac{2}{\gamma(\gamma - 1)}} \left(\frac{1 + \frac{\gamma - 1}{2} M_5}{1 + \sqrt{\frac{\gamma - 1}{2\gamma}}} \right) \quad (10)$$

This relation is a function only of \bar{A} and M_5 and is plotted in figure 5. As is apparent from the figures, the required value of $(a_4/a_5)_I$ increases with M_5 . More interesting, however, is the fact that the required sound speed ratio drops sharply as \bar{A} increases to a value of 10. Above $\bar{A} = 10$, the driver sound speed becomes relatively insensitive to changes in \bar{A} . In fact, as \bar{A} (i.e., M_e) becomes larger, $(a_4/a_5)_I$ approaches a limit independent of \bar{A} , given by

$$\left(\frac{a_4}{a_5}\right)_I = \left(\frac{\bar{\gamma} + 1}{2} \frac{\bar{\gamma} - 1}{2}\right)^{1/2} \sqrt{\frac{2}{\gamma(\gamma - 1)}} \left(\frac{1 + \frac{\gamma - 1}{2} M_5}{1 + \sqrt{\frac{\gamma - 1}{2\gamma}}} \right) \quad (11)$$

Also indicated in figure 5 are the values of a_4/a_5 at which $T_4/T_5 = 50, 25,$ and $10,$ the gases being calorically perfect helium and air in regions 4 and 5, respectively. It becomes apparent then that, for the helium air system with $\bar{A} \geq 10,$ $T \leq 4200^\circ \text{K}$ for $T_5 = 300^\circ \text{K}.$ These, with present arc discharge techniques, are relatively modest requirements.

With the use of equations (3), (6), and (10), the parameter Φ_I given by

$$\Phi_I = \frac{(p_4/p_5)_I}{(p_4/p_5)_O} = \left\{ \left[\frac{\bar{\gamma} + 1}{2} \left(1 + \frac{\bar{\gamma} - 1}{2} M_e^2 \right) \right]^{1/2} - \frac{\bar{\gamma} - 1}{2} M_e \right\}^{\frac{2\bar{\gamma}}{\bar{\gamma} - 1}} \quad (12)$$

is determined and is indicative of the relative change in the driver pressure required as a result of the nozzle addition to the basic expansion-tube configuration. Equation (12) is shown in figure 6 and is a function only of $\bar{A},$ this being a result of using the same value of a_4/a_5 in the expansion tube as in configuration I. As seen from figure 6, configuration I suffers large pressure disadvantages for nozzles of large $\bar{A}.$ These relative disadvantages become more severe if values of $a_4/a_5,$ larger than required by configuration I, are used in the expansion tube.

Several comments should be made at this point. First, in figure 6, for $\bar{A} = \widetilde{1.0} (\log_{10} \bar{A} = \bar{0})$ the basic expansion-tube process is not represented in general, even though the cross-sectional area is invariant. The process indicated in this fashion is the limit

$$M_e \rightarrow M_i = 1.0 \quad (13)$$

representing expansion-tube operation with the restriction that the driver gas is expanded only to sonic conditions. This is not a general restriction on expansion-tube operation and henceforth, for all configurations, curves labeled $\bar{A} = \widetilde{1.0}$ represent the limit described by equation (13), whereas those labeled $\bar{A} = 1.0$ denote the general expansion-tube cycle. Any exceptions to this are noted.

The asymptote indicated by the vertical line noted in figure 4 represents the expansion of the driver to the limiting state. In the limiting state, $p_3/p_4 \rightarrow 0$ and p_4 moves to infinity in an effort to raise the level of p_3 to the nonzero value of p_2 and to

maintain interface requirements. The net result for finite p_5 is to drive $(p_4/p_5)_0 \rightarrow \infty$. The limiting states for $(a_4/a_5)_0 = 10$ and 20 occur at values of M_5 given by

$$M_5 = \frac{2}{\gamma - 1} \left[\frac{2}{\gamma - 1} \left(\frac{a_4}{a_5} \right)_0 \sqrt{\frac{\gamma(\gamma - 1)}{2}} \left(1 + \sqrt{\frac{\gamma - 1}{2\gamma}} \right) - 1 \right] \quad (14)$$

and are well out of range for the conditions of interest herein.

Driver Requirements for Configuration II

From the preceding section, it becomes clear that configuration I will generally operate at a disadvantage, relative to the expansion tube, with regard to driver pressure. For $\bar{A} = 10^3$, the expansion tube is capable of operating at pressures 4 to 5 orders of magnitude lower than that required in configuration I. Driver sound speed requirements, however, are modest, and at low values of M_5 , quite low. However, if $(a_4/a_5)_{\bar{A}}$ is raised beyond those values required for a perfectly expanding nozzle, one would expect a flow requiring a backward-facing shock (fig. 1(b)) and possibly other unsteady waves in order to establish the interface conditions between 2 and 3e (fig. 1(b)). This adjusting wave system would imply driver pressures lower than those required for configuration I.

Consider first the relative magnitude of the nondimensional velocities u_2/a_5 and u_e/a_5 and of the pressures p_2/p_5 and p_e/p_5 . From equations (1a) and (4) applied across regions 2 to 5, the following expression is obtained:

$$\frac{u_2}{a_5} = \frac{1 + \frac{\gamma - 1}{2} M_5}{1 + \sqrt{\frac{\gamma - 1}{2\gamma}}} \sqrt{\frac{2}{\gamma(\gamma - 1)}} \quad (15)$$

The quantity u_e/a_5 may be written as

$$\frac{u_e}{a_5} = \left(\frac{a_4}{a_5} \right)_{\bar{A}} \left(\frac{a_i}{a_4} \right) \left(\frac{a_e}{a_i} \right) \left(\frac{u_e}{a_e} \right) \quad (16)$$

When substituting equations (1a) and (1b) into equation (16), it may be written as

$$\frac{u_e}{a_5} = \left(\frac{a_4}{a_5} \right)_{\bar{A}} M_e \left[\left(\frac{\bar{\gamma} + 1}{2} \right) \left(1 + \frac{\bar{\gamma} - 1}{2} M_e^2 \right) \right]^{-1/2} \quad (17)$$

Results of equations (15) and (17) are shown graphically in figure 7 in the form

$\frac{u_e}{a_5} = f\left[\left(\frac{a_4}{a_5}\right)_{\bar{A}}, \bar{A}\right]$. The ticks on the curves indicate the values of $(a_4/a_5)_{\bar{A}}$ at which the nozzle would be perfectly expanded ($u_e/a_5 = u_2/a_5$) for that particular value of \bar{A} and M_5 . If for a given value of \bar{A} and M_5 , $(a_4/a_5)_{\bar{A}}$ exceeds this value, the nozzle will be overexpanded since $u_e/a_5 > u_2/a_5$. From figure 7, it is apparent that for $(a_4/a_5)_{\bar{A}} \cong 11$, a modest sound speed requirement, the nozzle will be overexpanded for $M_5 = 50$, $\bar{A} \cong 10$.

When applying equations (1a) and (2a) across regions 2 and 5, the nondimensional pressure p_2/p_5 is

$$\frac{p_2}{p_5} = \frac{\left(1 + \frac{\gamma - 1}{2} M_5^2\right)^{\frac{2\gamma}{\gamma - 1}}}{1 + \sqrt{\frac{\gamma - 1}{2\gamma}}} \quad (18)$$

With the aid of equations (1a), (1b), and (2a), the quantity p_e/p_5 is given by

$$\frac{p_e}{p_5} = \left(\frac{p_4}{p_5}\right) \left(\frac{p_e}{p_i}\right) \left(\frac{p_i}{p_4}\right) = \frac{p_4}{p_5} \left(\frac{2}{\bar{\gamma} + 1}\right)^{\frac{\bar{\gamma}}{\bar{\gamma} - 1}} \left(1 + \frac{\bar{\gamma} - 1}{2} M_e^2\right) \quad (19)$$

The result of the combination of equations (18) and (19) is shown in figure 8 where the function $p_e/p_5 = f\left(\bar{A}, \frac{p_4}{p_5}\right)$ is shown plotted. Superposed on this plot are a family of vertical lines, each representing a value of M_5 . The intersection of the vertical lines with the lines of constant \bar{A} define the values of p_4/p_5 required for perfect expansion for that particular value of \bar{A} and M_5 . Values of p_4/p_5 lower than the perfect expansion value produce an overexpanded flow requiring a rearward-facing shock to adjust p_e/p_5 to the level of p_2/p_5 .

Figure 8 also makes clear the fact that, for the higher values of M_5 and \bar{A} , values of p_4/p_5 required to produce a perfectly expanded flow are too high. Operation in the overexpanded mode appears to be necessary.

The question to be considered is what type of adjusting waves is required. At this point, lengths and pressures involved are assumed to be such that the flow between the

primary shock and interface may be considered uniform. Driver conditions are then selected such that an upstream-facing shock wave, moving into the expanded driver gas, produces the adjustment required for the overexpansion. This process is indicated in figure 1(b) where p_{3e} denotes interface conditions in the driver gas.

Since $p_2 = p_{3e}$, the parameter $(p_4/p_5)_{II}$ may be written as

$$\left(\frac{p_4}{p_5}\right)_{II} = \left(\frac{p_4}{p_i}\right) \left(\frac{p_i}{p_e}\right) \left(\frac{p_e}{p_{3e}}\right) \left(\frac{p_2}{p_5}\right) \quad (20)$$

By dividing by $(p_4/p_5)_O$, the parameter Φ_{II} is defined as

$$\Phi_{II} \equiv \frac{(p_4/p_5)_{II}}{(p_4/p_5)_O} \quad (21)$$

The ratio p_{3e}/p_e in equation (20) is given from normal shock relations as

$$\frac{p_{3e}}{p_e} = 1 + \frac{2\bar{\gamma}}{\bar{\gamma} + 1} (M_{es}^2 - 1) \quad (22)$$

where

$$M_{es} = \frac{u_e + u_{es}}{a_e} \quad (23)$$

The adjusting shock velocity u_{es} relative to the tube is assumed positive in an upstream direction.

Appendix A shows that the required value of M_{es} for such a situation is given by the expression

$$M_{es} = \frac{\gamma + 1}{4} \zeta + \left[\left(\frac{\gamma + 1}{4} \zeta \right)^2 + 1 \right]^{1/2}$$

where

$$\zeta = \frac{u_e/a_5 - u_2/a_5}{(a_e/a_4)(a_4/a_5)\bar{A}}$$

and depends on $(a_4/a_5)\bar{A}$, M_5 , and \bar{A} .

In figure 9, the shock Mach number of the required adjusting shock is shown as a function of $(a_4/a_5)_{\bar{A}}$, M_5 , and \bar{A} . This plot was prepared with the use of equations (1a), (1b), (2a), (15), and (16) to evaluate ζ . Equation (A5) was then used to determine M_{es} .

As seen from figure 9, the adjusting shock Mach number decreases with increasing M_5 . In fact, for $(a_4/a_5)_{\bar{A}} = 5$ and 10, M_{es} assumes the value of unity thus indicating a perfect expansion within the M_5 range considered herein. The value of M_5 at which this occurs is given by the inverse of equation (10). For values of $(a_4/a_5)_{\bar{A}} > 10$, M_5 is out of range.

With the aid of equations (1), (2), (3), and (22), Φ_{II} may be determined for a given value of M_5 , \bar{A} , and $(a_4/a_5)_{\bar{A}}$. Values of this parameter are presented in figure 10 for the several values of $(a_4/a_5)_{\bar{A}}$ and \bar{A} .

The conclusion that significant reductions in driver pressure may be achieved for $\bar{A} \geq 10^2$ as a result of the overexpanded configuration may be drawn from figure 13. The costs of such gains are the larger values of $(a_4/a_5)_{\bar{A}}$ required (when compared with configuration I). These values lie within the expansion-tube range, however, and are tolerable.

One final point of interest is noted. For the curves for $(a_4/a_5)_{\bar{A}} = 5$ and 10, as those values of M_5 are approached at which $M_{es} \rightarrow 1.0$ (fig. 9) then configuration II becomes perfectly expanded. This condition is reflected in figure 10 by the upswing of those particular curves terminating at the proper value of M_5 given by the inverse of equation (10). The points of termination are joined by the near vertical curves shown in figure 10 labeled "Perfect expansion limit."

There must now be answered the question of when the adjusting shock wave is trapped in the nozzle. Such a situation would result in an unstarted nozzle, possibly generating strong upstream waves, and is not permissible. From equation (23) u_{es} , the wave velocity relative to the facility, is given by

$$u_{es} = M_{es} a_e - u_e \quad (24)$$

Since u_{es} is taken as positive in an upstream direction, it is required that $u_{es} \geq 0$. This inequality insures that the nozzle flow is not disturbed by the adjusting wave. Equation (24) may then be written

$$u_{es} a_e - u_e < 0 \quad (25)$$

or

$$M_{es} < M_e \quad (26)$$

Equation (26) is now the requirement to be satisfied. From equations (1), (2), (15), (16), (A4), (A5), and (26), values of M_5 required to avoid trapped shocks were determined for a range of \bar{A} and $(a_4/a_5)\bar{A}$. The results, shown in figure 11, ideally indicate the lowest values of M_5 which may be tolerated for a given value of \bar{A} and $(a_4/a_5)\bar{A}$. Application of these lower limits is indicated in figure 10 by the lines, labeled "Trapped shock limit," terminating the Φ_{II} curves at the lower values of M_5 . Before proceeding, it should be pointed out that the possibility of a third limiting curve exists. This limit (not shown here) would in practice occur at conditions where the adjusting shock causes boundary-layer separation possibly generating downstream waves that render the flow useless. It is believed that this limit occurs at values of M_5 larger than the trapped shock values; thus, the already small operating regime is further truncated.

Driver Requirements for Configuration III

Configuration III, investigated in a preliminary manner at the Arnold Engineering Development Center, whose wave and physical schematics are shown in figures 1(c) and 2(b), is assumed to operate by first expanding the shock-processed gas 2 steadily through the inserted nozzle to conditions e then unsteadily by the u - a expansion fan to test conditions 5, with interactions due to starting phenomena being neglected. The following analysis proceeds from this assumption.

The driver pressure parameter $(p_4/p_5)_{III}$ may be written in terms of the ratios

$$\left(\frac{p_4}{p_5}\right)_{III} = \left(\frac{p_4}{p_3}\right)\left(\frac{p_i}{p_e}\right)\left(\frac{p_e}{p_5}\right) \quad (27)$$

since

$$p_3 = p_2 = p_i \quad (28)$$

By utilizing the interface conditions along with equations (1a), (1b), (2a), (4), and (28), equation (27) may be expressed as

$$\left(\frac{p_4}{p_5}\right)_{\text{III}} = \frac{\left(\frac{1 + \frac{\gamma-1}{2}M_5}{1 + \frac{\gamma-1}{2}M_e}\right)^{\frac{2\gamma}{\gamma-1}} \left(\frac{1 + \frac{\gamma-1}{2}M_e^2}{\frac{\gamma+1}{\gamma}}\right)^{\frac{\gamma}{\gamma-1}}}{\left[1 - \frac{\bar{\gamma}-1}{2} \sqrt{\frac{2}{\gamma(\gamma-1)}} \frac{1}{(a_4/a_5)\bar{A}} \left(\frac{1 + \frac{\gamma-1}{2}M_e^2}{\frac{\gamma+1}{\gamma}}\right)^{1/2} \left(\frac{1 + \frac{\gamma-1}{2}M_5}{1 + \frac{\gamma-1}{2}M_e}\right)\right]^{\frac{2\bar{\gamma}}{\bar{\gamma}-1}}} \quad (29)$$

Dividing equation (29) by equation (3) (with $(a_4/a_5)\bar{A} = (a_4/a_5)_0$) results in the ratio Φ_{III}

$$\Phi_{\text{III}} = \frac{(p_4/p_5)_{\text{III}}}{(p_4/p_5)_0} = f\left(M_5, \left(\frac{a_4}{a_5}\right)\bar{A}, \bar{A}\right) \quad (30)$$

This ratio is shown graphically in figure 12 for various values of the independent variables. As is evident from this figure, there are several limitations, denoted by the labeled vertical lines, which restrict the range of operation of this configuration. The indicated asymptotes represent limit lines to which the curves for $\bar{A} = 10, 10^2, \text{ and } 10^3$, for $(a_4/a_5)\bar{A} = 5$, tend. This limit is a result of the limiting state being reached by configuration III resulting in $p_4/p_3 \rightarrow \infty$. A comparison of figure 12 with figure 4 indicates that this limiting state is achieved at a smaller value of M_5 for configuration III than that for the basic expansion tube. The last limitation, indicated in figure 12, represents the Mach number to which the inlet flow expands when passed through a nozzle with $\bar{A} = 10^3$; consequently, this is the lowest value of M_5 which can be achieved with this configuration. This limitation presupposes an inlet Mach number given by strong shock approximations (eq. (4)) with $\gamma = 1.4$.

Comparison of figure 12 with figures 6 and 10 indicates that in some operating areas, configuration III is the facility with the least penalty in regard to the driver pressure but, nonetheless, there remains a penalty of several orders of magnitude in p_4 when compared with the constant-area tube. Further discussion is presented in later sections.

Intermediate-Chamber Pressure for Configurations I, II, and III

The pressure ratio across the primary shock may be given as

$$\frac{p_2}{p_1} = \left(\frac{p_2}{p_e}\right)\left(\frac{p_e}{p_5}\right)\left(\frac{p_5}{p_1}\right) = \frac{2\gamma}{\gamma+1} M_{S1}^2 \quad (31)$$

with the strong shock assumptions. If a nozzle is assumed to be present in the configuration, the quantity p_1/p_5 is

$$\frac{p_1}{p_5} = \frac{\frac{p_i}{p_e} \frac{p_e}{p_5}}{\frac{2\gamma}{\gamma+1} M_{S1}^2} \quad (32)$$

By applying the analysis in appendix A, it may be determined that

$$M_{S1} = \frac{\gamma+1}{2} \sqrt{\frac{2}{\gamma(\gamma-1)}} \left(\frac{a_i}{a_e}\right)\left(\frac{a_e}{a_5}\right)\left(\frac{a_5}{a_1}\right) \quad (33)$$

where the strong shock approximation has been employed. The intermediate-chamber parameter $\frac{p_1}{p_5} \left(\frac{a_5}{a_1}\right)^2$, evaluated with the aid of equations (1a), (1b), (2a), and (33), is shown in figure 13 as a function of \bar{A} and M_5 and increases with both.

At this point, it should be noted that once the primary shock wave is set in motion, the problem is one of a constant area for configurations I and II. Hence, the curve for $\bar{A} = 1.0$ in figure 13 is valid for these configurations as well as for the expansion tube. However, since the area change does affect configuration III, curves for various values of \bar{A} are shown in figure 13.

Acceleration-Chamber Pressure for Configurations I, II, and III

The acceleration-chamber pressure parameter $\frac{p_{10}}{p_5} \left(\frac{a_5}{a_{10}}\right)^2$ may be determined for the present configurations by using the analysis of appendix A. The resulting relation given by

$$\frac{p_{10}}{p_5} \left(\frac{a_5}{a_{10}}\right)^2 = \frac{2}{\bar{\gamma}(\bar{\gamma}+1) M_5^2} \quad (34)$$

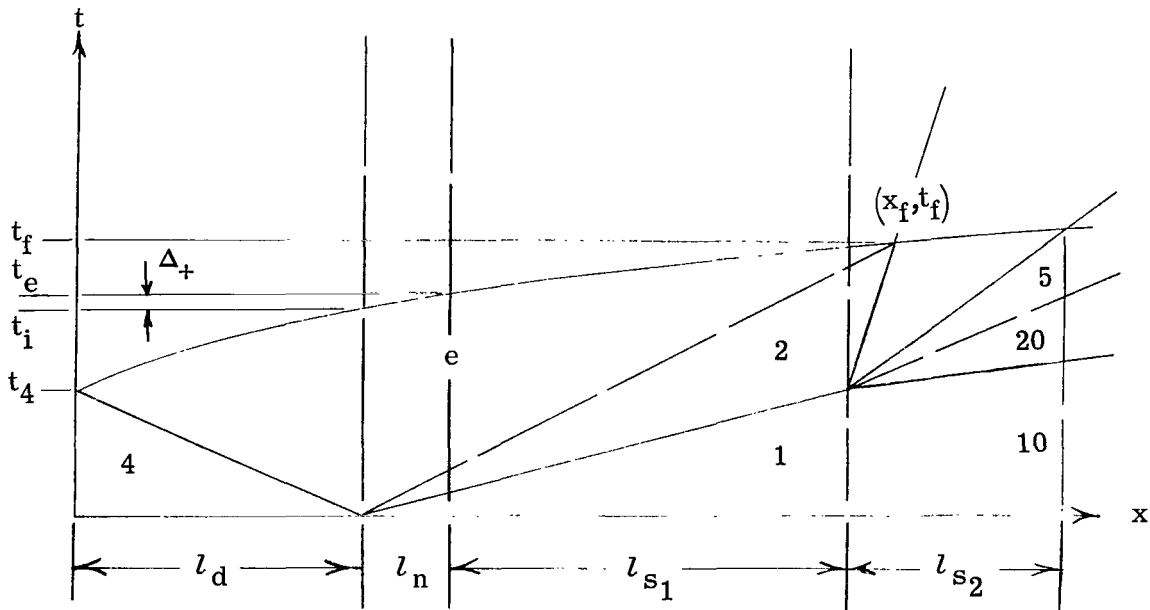
is shown in figure 14 in inverted form. Vacuum requirements in the accelerating section are reduced with decreasing a_5/a_{10} .

Finally, equation (34) is valid for all configurations including the expansion tube since once the secondary shock has been set in motion the process is a constant area one.

Component Lengths

The determination of the component lengths and their required variation with the independent operating parameters to insure maximum operational efficiency are discussed in this section. In order to secure explicit solutions for the length ratios of interest, it is necessary to neglect nozzle starting effects as well as variation of interface and shock velocity in nozzles. These assumptions, though contrary to the physical situation, allow solutions from which valuable information, not easily obtained otherwise, can be determined.

Configuration I.- For configuration I the optimum lengths occur when the reflected head of the driver expansion, the driver-driven gas interface, and the head of the secondary expansion which processes the test gas coalesce at a given point on the x-t diagram (fig. 1). Selecting a driver longer than that necessary to achieve this wave configuration results in increasing the energy required in the driver with no increase in testing time. Decreasing the driver lengths, however, results in a truncated test time. Hence, the wave schematic shown in figure 1(a) represents the most efficient operation of the device and is used as a criterion for determining relative component lengths, that is, l_d/l_{s1} , l_n/l_{s1} , and l_{s2}/l_{s1} . The analysis is greatly facilitated with the use of sketch 1 which follows:



Sketch 1

According to sketch 1, the following equation may be written:

$$t_e = t_4 \left(\frac{t_i}{t_4} \right) + \Delta_+ \quad (35)$$

where, according to reference 3,

$$\left. \begin{aligned} t_4 &= \frac{l_d}{a_4} \\ \frac{t_i}{t_4} &= \left(\frac{a_4}{a_i} \right)^{\frac{\bar{\gamma}+1}{2(\bar{\gamma}-1)}} \end{aligned} \right\} \quad (36)$$

Since conditions i are sonic, equations (1a) and (36) may be combined to give

$$t_4 \left(\frac{t_i}{t_4} \right) = \frac{l_d}{a_4} \left(\frac{\bar{\gamma}+1}{2} \right)^{\frac{\bar{\gamma}+1}{2(\bar{\gamma}-1)}} \quad (37)$$

The last term on the right of equation (35) may be given by

$$\Delta_+ = \xi_+ \frac{l_n}{a_e} \quad (38)$$

where

$$\xi_{+,-,f} = (t_e - t_i)_{+,-,f} \left(\frac{a_e}{l_n} \right) \quad (39)$$

may be evaluated from reference 2, for a conical nozzle, with \bar{A} and γ known. The time t_f is now determined as a function of the known parameters. In order to do this, it is necessary to assume that the shock and interface velocities are constant despite the presence of the nozzle. This assumption, which is discussed in the section "General Considerations," allows the following equations to be written:

$$\left. \begin{aligned} x_f &= u_2 t_f \\ x_f &= l_{s1} + l_n + (u_2 - a_2) \left(t_f - \frac{l_{s1} + l_n}{u_2} \frac{2}{\gamma + 1} \right) \end{aligned} \right\} \quad (40)$$

Solving equations (40) for t_f with the use of equation (9) gives

$$t_f = \frac{l_{s1} + l_n}{a_1} \frac{a_1}{a_5} \left(\frac{1 + \frac{\gamma-1}{2} M_2}{1 + \frac{\gamma-1}{2} M_5} \right) \left(\frac{\gamma-1}{\gamma+1} + \frac{2}{\gamma+1} \frac{1}{M_2} \right) \quad (41)$$

Finally, in order to insure coalescence of the desired wave fronts, the following equation must be satisfied

$$u_2 t_f = l_n + (u_e + a_e)(t_f - t_e) \quad (42)$$

Substituting equations (10), (35), (37), (38), and (41) into equation (42) gives the following expression for $\left(\frac{l_d}{l_{s1}} \right)_I$:

$$\left(\frac{l_d}{l_{s1}} \right)_I = \left(\frac{l_d}{l_{s1}} \right)_{I_m} \left(1 + \frac{l_n}{l_{s1}} \right) - \frac{l_n}{l_{s1}} \frac{\beta}{(M_e + 1) \left(\frac{\bar{\gamma} + 1}{2} \right) \frac{\bar{\gamma} + 1}{2(\bar{\gamma} - 1)}} \quad (43)$$

where $\left(\frac{l_d}{l_{s1}} \right)_{I_m}$ is the value of $\left(\frac{l_d}{l_{s1}} \right)_I$ for $\frac{l_n}{l_{s1}} = 0$ and is expressed by the functional relation

$$\left(\frac{l_d}{l_{s1}} \right)_{I_m} = \frac{\frac{1}{M_e} \sqrt{\frac{2}{\gamma(\gamma-1)}} \left[\frac{\bar{\gamma} + 1}{2} \left(1 + \frac{\bar{\gamma} - 1}{2} M_e^2 \right) \right]^{1/2} \left[\frac{\gamma - 1}{\gamma + 1} + \frac{2}{\gamma + 1} \sqrt{\frac{\gamma(\gamma-1)}{2}} \right]}{(M_e + 1) \left(\frac{\bar{\gamma} + 1}{2} \right) \frac{\bar{\gamma} + 1}{2(\bar{\gamma} - 1)}} \quad (44)$$

The quantity β is given by

$$\beta = \left[\left(\frac{\bar{\gamma} + 1}{2} \right) \left(1 + \frac{\bar{\gamma} - 1}{2} M_e^2 \right) \right]^{1/2} \left[\xi_+ (M_e + 1) - 1 \right] \quad (45)$$

with $\xi_+ \rightarrow \frac{1}{M_e + 1}$ as $\bar{A} \rightarrow \widehat{1.0}$; hence, $\beta \rightarrow 0$. For $\bar{A} = \widehat{1.0}$, equation (44) reduces to

$$\left(\frac{l_d}{l_{s1}}\right)_{I_m} = \frac{\sqrt{\frac{2}{\gamma(\gamma-1)}\left(\frac{\bar{\gamma}+1}{2}\right)\left[\frac{\gamma-1}{\gamma+1} + \frac{2}{\gamma+1}\sqrt{\frac{\gamma(\gamma-1)}{2}}\right]}}{2\left(\frac{\gamma+1}{2}\right)^{\frac{\bar{\gamma}+1}{2(\bar{\gamma}-1)}}} \quad (46)$$

and assumes a value $\left(l_d/l_{s1}\right)_{I_m} = 0.431$ for $\gamma = 1.4$ and $\bar{\gamma} = 1.67$.

Equation (43) is presented graphically in figure 15 for various values of \bar{A} and l_n/l_{s1} . The parameter $\left(l_d/l_{s1}\right)_I$ decreases with increasing \bar{A} and decreasing l_n/l_{s1} . For purposes of comparison, the length ratio $\left(l_d/l_{s1}\right)_{\bar{A}=1.0}$ is shown superposed in figure 15. This ratio was computed with the aid of the following equation:

$$\left(\frac{l_d}{l_{s1}}\right)_{\bar{A}=1.0} = \frac{1}{2}\left(\frac{a_4}{a_5}\right)_o \left(\frac{1 + \sqrt{\frac{\gamma-1}{2\gamma}}}{1 + \frac{\gamma-1}{2}M_5}\right) \left[\frac{\gamma-1}{\gamma+1} + \frac{2}{\gamma+1}\sqrt{\frac{\gamma(\gamma-1)}{2}}\right] \left[1 - \frac{\bar{\gamma}-1}{2}\sqrt{\frac{2}{\gamma(\gamma-1)}}\left(\frac{1 + \frac{\gamma-1}{2}M_5}{1 + \sqrt{\frac{\gamma-1}{2\gamma}}}\right)\left(\frac{a_4}{a_5}\right)_o\right]^{\frac{\bar{\gamma}+1}{2(\bar{\gamma}-1)}} \quad (47)$$

The derivation of equation (47) is not presented because it is similar to that of equation (43). Computations using this equation were made at the same value of $(a_4/a_5)_o$ as required for configuration I. (See eq. (10).) As would be expected, $\left(l_d/l_{s1}\right)_I < \left(l_d/l_{s1}\right)_{\bar{A}=1.0}$ for $\bar{A} > 1.0$ and $l_n/l_{s1} = 0$. In addition, it is clear from figure 15 that $\left(l_d/l_{s1}\right)_I < \left(l_d/l_{s1}\right)_{\bar{A}=1.0}$ for $\bar{A} > 40$ and $l_n/l_{s1} \neq 0$.

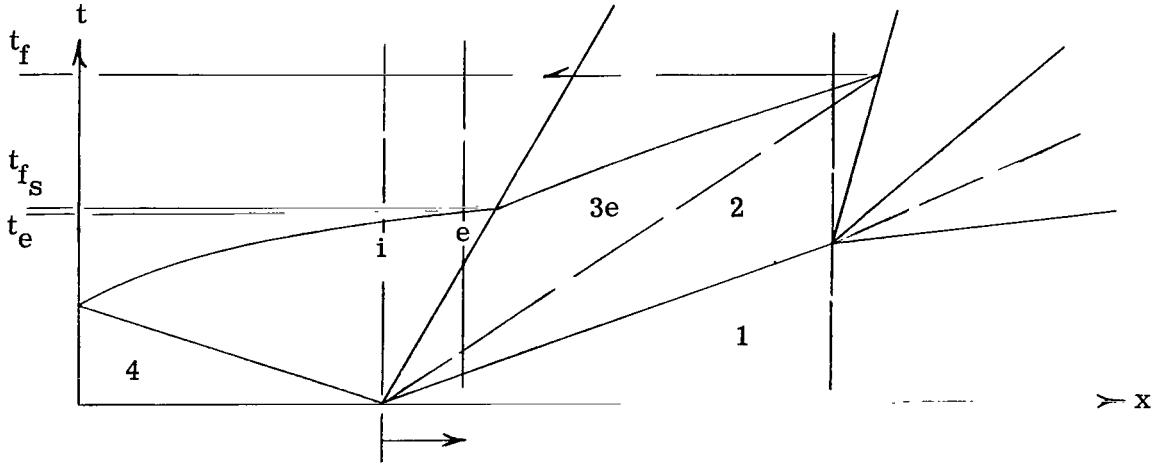
The length of the acceleration chamber l_{s2} is determined such that maximum test time is available. The governing equation may be determined from equation (63) of reference 2 and is given by

$$\frac{l_{s2}}{l_{s1}}\left(1 + \frac{l_n}{l_{s1}}\right)^{-1} = \frac{\gamma-1}{\gamma+1}(M_5 - 1)\left(\frac{1 + \frac{\gamma-1}{2}M_5}{1 + \frac{\gamma-1}{2}M_2}\right)^{\frac{3-\gamma}{2(\gamma-1)}} \quad (48)$$

where account has been taken of present nozzle length effects and the entropy gradients in region 2 have been neglected. Values of M_2 are given by equation (4). Equation (48) is shown graphically in figure 16 and is valid for arbitrary values of \bar{A} for configurations I and II as well as the expansion tube. As can be seen $l_{s2}/l_{s1} \sim 0(10 - 10^3)$, hence,

considerable lengths may be involved for reasonably sized intermediate sections. A more complete discussion of this aspect is given in reference 1.

Configuration II.- The procedure for configuration I is now repeated for configuration II. The following sketch (sketch 2) is helpful:



Sketch 2

The procedure is the same except that account must now be taken of the fact that the reflected head of the expansion encounters the backward facing shock and alters its speed.

Writing an expression for the axial coordinate of the adjusting shock wave and equating it to that for the $u + a$ characteristic results in the following expression:

$$-u_{es}t_{fs} = l_n + (u_e + a_e)(t_{fs} - t_e) \quad (49)$$

Solving equation (49) for the time at which the two waves intersect t_{fs} gives

$$t_{fs} = \frac{l_n - (u_e + a_e)t_e}{-[u_{es} + (u_e + a_e)]} \quad (50)$$

The negative sign is required on the left-hand side of equation (48) since u_s is positive in an upstream direction.

If the displacement equation of the interface

$$x = u_2t \quad (51)$$

and of the $u + a$ wave after intersection with the adjusting shock wave

$$x = -u_{es} t_f + (u_{3e} + a_{2e})(t - t_{fs}) \quad (52)$$

are written, the conditions for most efficient performance of the device may be determined by setting $t = t_f$ and equating equations (51) and (52). This operation and the substitution of equations (35), (37), (38), (41), and (50) results in

$$\left(\frac{l_d}{l_{s1}}\right)_{\Pi} = \left(\frac{l_d}{l_{s1}}\right)_{\Pi_m} \left(1 + \frac{l_n}{l_{s1}}\right) - \frac{l_n}{l_{s1}} \frac{\beta}{(M_e + 1) \left(\frac{\bar{\gamma} + 1}{2}\right)^{\frac{\bar{\gamma} + 1}{2(\bar{\gamma} - 1)}}} \quad (53)$$

where

$$\left(\frac{l_d}{l_{s1}}\right)_{\Pi_m} = \frac{\left(\frac{a_4}{a_5}\right)_{\bar{A}} \left(1 + \sqrt{\frac{\gamma - 1}{2\gamma}}\right) \left[\frac{\gamma - 1}{\gamma + 1} + \frac{2}{\gamma + 1} \sqrt{\frac{\gamma(\gamma - 1)}{2}}\right] \frac{M_{es} + 1}{M_{3e} + 1}}{(M_e + 1) \left(\frac{\bar{\gamma} + 1}{2}\right)^{\frac{\bar{\gamma} + 1}{2(\bar{\gamma} - 1)}}} \quad (54)$$

Shown plotted in figure 17 is the parameter

$$\left[\left(\frac{l_d}{l_{s1}}\right)_{\Pi} + \frac{l_n}{l_{s1}} \frac{\beta}{(M_e + 1) \left(\frac{\bar{\gamma} + 1}{2}\right)^{\frac{\bar{\gamma} + 1}{2(\bar{\gamma} - 1)}}} \right] \left(1 + \frac{l_n}{l_{s1}}\right)^{-1}$$

from which $\left(l_d/l_{s1}\right)_{\Pi}$ may be determined. Figure 17 includes, for comparison purposes, a curve representing normal expansion-tube operation, denoted by $\bar{A} = 1.0$. For this case, the ordinate is simply $\left(l_d/l_{s1}\right)_{\bar{A}=1.0}$ since $l_n/l_{s1} = 0$. The quantity $\left(l_d/l_{s1}\right)_{\bar{A}=1.0}$ was determined from equation (47).

From figure 17, trends become apparent and it is seen that the addition of a nozzle to the expansion tube and its operation in the mode of configuration II results in a driver of shorter length, this length decreasing with increasing \bar{A} and decreasing $(a_4/a_5)_{\bar{A}}$.

The driver length for configuration I is smaller over most operating ranges than that for the expansion tube or configuration II. (Compare figs. 15 and 17.) This result is

primarily due to the lower sound speeds required by configuration I coupled with the relative efficiencies of the steady and unsteady supersonic expansions in configuration I and the expansion tube, respectively.

It should be pointed out that in figure 17 the curves for $\bar{A} = 10, 10^2, \text{ and } 10^3$ are terminated by a dashed line at the values of M_5 which represent the perfectly expanded states of configuration I.

Configuration III.- Consider now configuration III. From figure 1(c), it is apparent that the driver length should be tailored so that the expanded helium driver gas and air interface and the head of the reflected nonsteady driver expansion fan coalesce at the nozzle entrance. A larger or shorter driver will move the operation of the device off the point of maximum efficiency.

The analysis necessary to determine these lengths is similar to that required for the other configurations except that there is no nozzle to contend with and the point of intersection of the interface and expansion wave is fixed. The equation of motion for the interface is given by equation (51) which is

$$x = u_2 t$$

whereas that for the $u + a$ wave resulting from the reflected expansion is

$$x = x_3 + (u_3 + a_3)(t - t_3) \quad (55)$$

where x_3 and t_3 define the point at which the first reflected characteristic enters the uniform region 3. Note that x_3 is given by the relation

$$x_3 = (u_3 - a_3)t_3 \quad (56)$$

Setting $x = l_{s1}$ in equation (50), the time of interface arrival at the end of the driven section t_f is determined. Using this time, equation (56) and $x = l_{s1}$ in equation (55), the following expression is obtained:

$$l_{s1} = 2u_3 t_3 \quad (57)$$

Applying equations (36) across the unsteady fan, region 4 to 3, t_3 may be determined and used in equation (57) to yield the desired expression for $(l_d/l_{s1})_{III}$, which is

$$\left(\frac{l_d}{l_{s1}}\right)_{\text{III}} = \frac{1}{2} \frac{1}{\frac{u_2}{a_4}} \left(1 - \frac{\bar{\gamma} - 1}{2} \frac{u_2}{a_4}\right)^{\frac{\bar{\gamma}+1}{2(\bar{\gamma}-1)}} \quad (58)$$

where

$$\frac{u_2}{a_4} = \sqrt{\frac{2}{\gamma(\gamma-1)}} \left(\frac{1 + \frac{\bar{\gamma} - 1}{2} M_e^2}{\frac{\gamma + 1}{\gamma}}\right)^{1/2} \left(\frac{1 + \frac{\gamma - 1}{2} M_5}{1 + \frac{\gamma - 1}{2} M_e}\right) \frac{1}{(a_4/a_5)_{\bar{A}}} \quad (59)$$

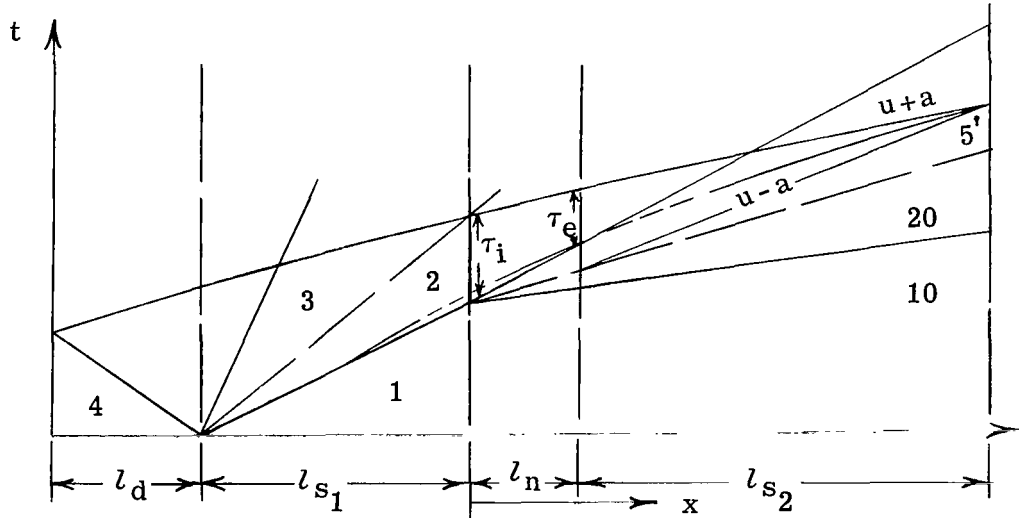
using the strong shock approximation, steady and unsteady flow equations.

Hence, with this information, $(l_d/l_{s1})_{\text{III}}$ is found as a function of \bar{A} , M_5 , and $(a_4/a_5)_{\bar{A}}$. Equation (58) is presented in figure 18 for a range of parameters, the dashed line labeled $\bar{A} = 1.0$ representing the parameter for normal expansion tube operation. The four vertical dashed lines of figure 18(a) represent the values of M_5 at which $(l_d/l_{s1})_{\text{III}} \rightarrow 0$, a result of achieving the limiting state in the driver expansion. From figure 18, it is apparent that significant reductions in the driver to intermediate-chamber length ratio may be realized when compared to the expansion tube. The magnitude of these benefits decreases with increasing $(a_4/a_5)_{\bar{A}}$.

It is now desirable to determine the required length of the acceleration chamber, l_{s2} . The analysis necessary is more easily understood after a consideration of figure 19, an $x-t$ representation of the unsteady wave processes occurring in the nozzle and acceleration chamber of configuration III. Shown are the primary and secondary shock waves and interfaces, the unsteady $u - a$ expansion fan (resulting in part from the motion of the secondary interface through the nozzle), a particle path, and the $u + a$ characteristic generated by the entrance of the primary interface in the nozzle.

Consideration of this figure reveals two major points of interest. The first is that particles entering the nonsteady fan prior to its exit from the nozzle may not be considered as suitable for testing purposes. Such particles, entering the fan at different times within the nozzle, experience different thermodynamic histories and hence, upon exiting from the expansion, have variable thermodynamic and flow properties. This flow is denoted by conditions 5'. Particles entering the unsteady expansion after its exit from the nozzle, when allowed to move entirely through the expansion, experience identical flow and thermodynamic histories. This mass flow is used for testing purposes and is denoted by conditions 5.

The second point of interest is simply that for a given value of l_{s2} , l_{s1} , or l_d there is a maximum nozzle length, which if exceeded allows no usable test flow at the test section (end of l_{s2}). This occurs when the nozzle length is such that the first reflected expansion characteristic, traveling with a velocity $u + a$, coalesces with the first usable test particle and the last expansion characteristic of the secondary fan at the end of l_{s2} . It is clear that to produce usable test time nozzles shorter than this limiting length must be used. The situation for zero test time ($\tau_5 = 0$) is indicated in the following sketch (sketch 3):



Sketch 3

Solutions for this limiting or maximum nozzle length are presented later.

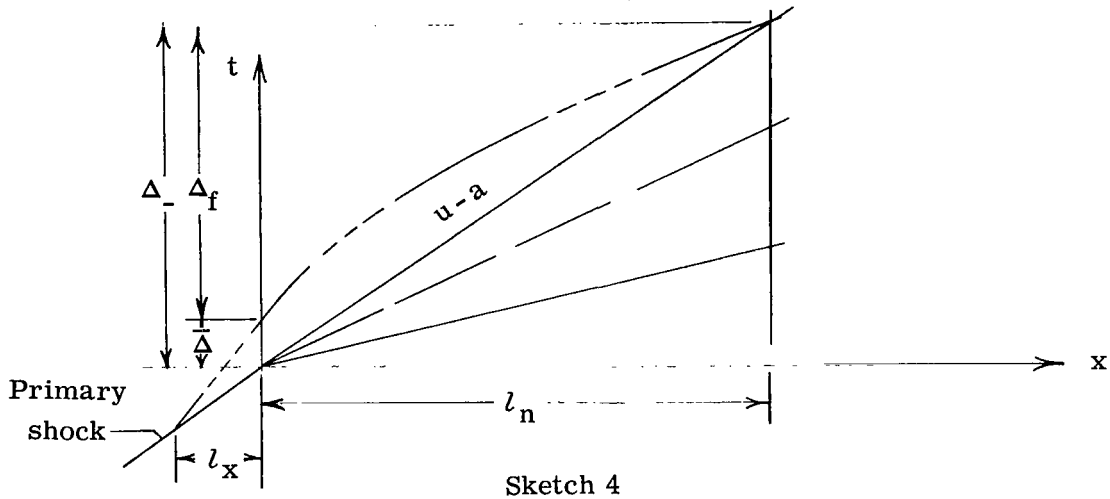
Now for a given value of l_n , ignoring for a moment the leading $u + a$ wave, the question to be answered is what value of l_{s2} is required to produce usable test time. As seen from figure 19, if l_{s2} is excessively short, those particles suitable for test purposes may not exit from the fan before passing the observation station. Consequently, no uniform region of flow exists. An exact analysis of this problem would require a difficult unsteady characteristic solution beyond the scope of this paper. In order to make possible analytical solutions, the following approximations are made:

- (1) Conditions $5 \approx 5'$ for this aspect of the analysis
- (2) Interactions between the secondary shock and its trailing interface are weak and may be neglected
- (3) Effects of the above interactions are not transmitted to regions $5'$ or 5
- (4) The unsteady expansion for, after exiting from the nozzle, may be treated as centered

These approximations are discussed in a later section.

The question raised previously with regard to l_{S_2} is now approached by utilizing a mass-flow analysis. Let the mass of gas contained in the slug of length l_x (fig. 19) which enters the unsteady expansion wave during passage through the nozzle be unacceptable for test purposes. This unacceptable mass of gas is compared to the mass passing the end of the acceleration chamber in the time interval τ' between the arrival of the interface and the last $u-a$ characteristic of the secondary expansion. From a comparison of these masses for specified parameters, that is, $\bar{\Delta}$, M_5 , and l_{S_2}/l_n , it can be determined whether any useful test time exists and, if so, how much.

For clarification of the following derivation, consider the following sketch:



It is first necessary to determine l_x . The quantity $\bar{\Delta}$ may be defined as

$$\bar{\Delta} \equiv l_x \left(\frac{1}{u_2} - \frac{1}{u_{S_1}} \right) = \Delta_- - \Delta_f \quad (60)$$

Solving for l_x with continuity and the strong shock approximations gives

$$l_x = \bar{\Delta} \frac{\gamma + 1}{\gamma - 1} u_2 = (\Delta_- - \Delta_f) \frac{\gamma + 1}{\gamma - 1} u_2 \quad (61)$$

where the quantity $(\Delta_- - \Delta_f)$ may be written as follows

$$\Delta_- - \Delta_f = (\xi_- - \xi_f) \frac{l_n}{a_e} \quad (62)$$

with ξ_- and ξ_f being evaluated once again for a conical nozzle with the use of reference 2. With equations (61) and (62) the mass of slug is given by

$$m_x = \rho_1 A_i \frac{\gamma + 1}{\gamma - 1} u_2 (\xi_- - \xi_f) \frac{l_n}{a_e} \quad (63)$$

The mass passing the end of the acceleration chamber in the interval τ' is

$$m_5 = \rho_5 u_5 A_e \tau' \quad (64)$$

where

$$\tau' = \frac{l_{s2}}{a_5} \frac{1}{M_5 (M_5 - 1)} \quad (65)$$

If $\psi = m_x/m_5$, the following expression may be written

$$\psi = \frac{\rho_2}{\rho_e} \frac{\rho_e}{\rho_5} \frac{1}{\bar{A}} \frac{1}{l_{s2}/l_n} (\xi_- - \xi_+) \frac{a_2}{a_e} \sqrt{\frac{2}{\gamma(\gamma - 1)}} (M_5 - 1) \quad (66)$$

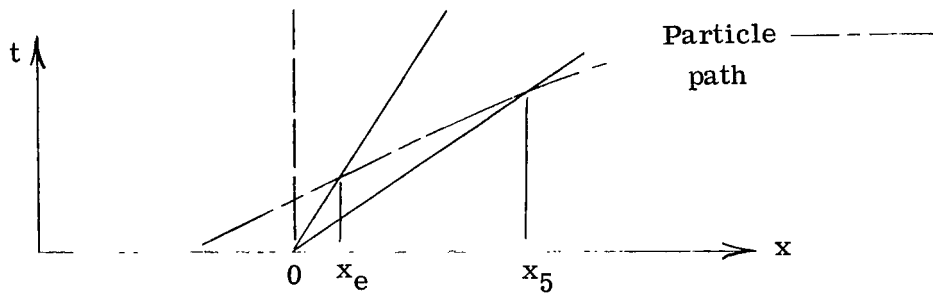
Substituting equations (1a), (1b), and (2b) into equation (66) yields

$$\frac{l_{s2}}{l_n} \psi = \frac{1}{\bar{A}} \sqrt{\frac{2}{\gamma(\gamma - 1)}} \left(\frac{1 + \frac{\gamma - 1}{2} M_e^2}{\frac{\gamma + 1}{\gamma}} \right)^{\frac{\gamma + 1}{2(\gamma - 1)}} \left(\frac{1 + \frac{\gamma - 1}{2} M_5}{1 + \frac{\gamma - 1}{2} M_e} \right)^{\frac{2}{\gamma - 1}} (M_5 - 1) (\xi_- - \xi_f) \quad (67)$$

Equation (67) is presented in figure 20. For most of the operating range, the parameter $(l_{s2}/l_n)\psi$ is greater than unity by several orders of magnitude. Recalling the definition of ψ , it is realized that in order to have any usable test time, l_{s2}/l_n must be a value such that ψ is determined to be less than unity. The conclusion is then, that for usable test time, the parameter l_{s2}/l_n must be of the order 10^2 to 10^4 for $M_5 \gtrsim 30$. For realistic nozzle lengths, this results in values of l_{s2} which are untenable. From figure 20 the observation is that the situation worsens for decreasing \bar{A} , the curve for $\bar{A} = 1.0$ representing not the expansion tube but the solution of equation (67) as $\bar{A} \rightarrow 1.0$.

With regard to the effect of the assumption that state 5 \approx 5', it is noted from equation (67) that $(l_{s2}/l_n)\psi \approx (M_5)^{\frac{\gamma + 1}{\gamma - 1}}$; hence, an overestimation of M_5 by 30 percent would raise $(l_{s2}/l_n)\psi$ by a factor of 5. It is unlikely that conditions 5' would deviate by more than 30 percent from 5; however, if such errors were present, l_{s2} would still be excessively long.

In order to make more clear the reason for the large lengths involved, the movement of a flow particle through a simple centered unsteady expansion is examined. In the following analysis, subscripts e and 5 denote, respectively, the conditions of the particle when entering and exiting from the expansion represented in the following sketch:



Sketch 5

The following derivation of the governing equation for the particle motion

$$\frac{x_5}{x_e} = \frac{M_5 - 1}{M_e - 1} \left(\frac{1 + \frac{\gamma - 1}{2} M_5}{1 + \frac{\gamma - 1}{2} M_e} \right)^{\frac{2}{\gamma - 1}} \quad (68)$$

is similar to that of equation (16) of reference 7 which describes the motion of a P characteristic through a u - a expansion. Equation (68) is shown in figure 21 for a range of parameters. Those values of M_e selected represent those existing at the exit of a nozzle with area ratio \bar{A} , $\gamma = 1.4$, and inlet Mach number, $M_i = 1.89$. From figure 21, this ratio is seen to be extremely large indicating that flow particles moving through an unsteady fan require considerable distances before emerging into the uniform flow region 5. This is especially true when $M_5 \gg 1$. It is precisely this effect that requires the large values of l_{s2} in order to achieve a usable test time in configuration III.

At this point, the evaluation of the effect that the u + a wave system has on the length parameter l_n/l_{s1} is necessary. Briefly, l_n/l_{s1} is evaluated under the constraint that it be a value such that the zero test time situation discussed previously and pictured in sketch 3 prevails at all conditions. Larger values of l_n/l_{s1} permit no usable test time regardless of l_{s2} . Shorter values allow test time to establish itself. Consequently, evaluating l_n/l_{s1} for a given value of l_{s1} and $\tau_5 = 0$ establishes a useful maximum value for l_n/l_{s1} which must not be exceeded or equaled if finite test time is desired. From the derivation in appendix B the relationship expressing this limiting value of $(l_n/l_{s1})_{III}$ is given by equation (B7) which is

$$\left(\frac{l_n}{l_{s1}}\right)_{III} = \frac{\left(\frac{\gamma+1}{\gamma}\right)^{1/2} \left[\frac{\gamma(\gamma-1)}{2}\right]^{1/2} \left(\frac{\gamma-1}{\gamma+1}\right)^{1/2} (M_e+1)(M_e-1)}{\frac{l_{s2}}{l_n} \tilde{\psi} \left[\frac{\frac{M_5-1}{M_e-1} \left(1 + \frac{\gamma-1}{2} M_5\right)^{\frac{\gamma+1}{2(\gamma-1)}}}{\left(1 + \frac{\gamma-1}{2} M_e\right)} - 1 \right] + \frac{2}{\gamma-1} \left(\frac{M_5-1}{M_e-1}\right)^{\gamma-1} - 1} + \frac{1}{2}(\xi_- - \xi_+)(M_e^2 - 1)$$

and depends on \bar{A} and M_5 . The parameters ξ_- and ξ_+ are evaluated according to reference 2, whereas $(l_{s2}/l_n)\tilde{\psi}$ is determined from figure 20. The tilde notation for ψ indicates $\psi = 1.0$, the value assumed when the first usable particle exists from the unsteady fan precisely at the end of l_{s2} , the situation prescribed herein.

Equation (B7) is shown in figure 22, with the curve for $\bar{A} = 1.0$ representing the limit of equation (B7) as $M_e \rightarrow M_i$, not expansion-tube operation. It is clear from this figure that the maximum permissible nozzle lengths are, for the most part, small when compared to l_{s1} . In fact, $(l_n/l_{s1})_{III}$ is so small that, for reasonable values of l_{s1} , the steady flow expansion characteristics may often extend past the nozzle exit before processing the center-line flow.

A second consideration is that the flow, if expanded through a large \bar{A} in such short lengths, surely is not one dimensional or even a close approximation to it. Consequently, a careful evaluation of the effect of the recompression shock waves generated at the juncture of the conical nozzle and the accelerating section must be made. These waves could easily be detrimental to the test flow.

DISCUSSION

General Considerations

At this point, the major assumptions employed in the foregoing analysis will be reiterated and briefly commented on with regard to their purpose and validity as follows:

(1) All gases were considered calorically perfect. This assumption permits closed-form solutions while maintaining a physical model reasonably close to that which would be observed. Such solutions are invaluable in the assessment of trends and the emphasizing of salient points.

(2) All shock waves with the exception of the adjusting shocks, were assumed to be strong. This is a commonly made assumption in shock-tube work resulting in more facile solutions with little error.

(3) Shock wave and interface speeds through nozzles with arbitrary \bar{A} were taken to be invariant. In addition, it was assumed that nonsteady interactions between shock waves and trailing entropy discontinuities, due to passage through nozzles, were negligible. Without these assumptions, analytical solutions of the passage of waves and discontinuities of various types through nozzles would be impossible to obtain. It was felt that errors which must result from such assumptions may be held to acceptable levels if $(l_n/l_{s1})_{I,II} \cong 0(10^{-1})$ and $(l_n/l_{s2})_{III} \cong 0(10^{-1})$. This results in average wave and interface velocities relatively unaffected by variations within the nozzle. Trends sought and determined under these restrictions are felt to be reasonably accurate.

(4) Conditions 5' are approximately equal to conditions 5 for configuration III. This is an outgrowth of assumption (3) and is necessary for an analytical solution for l_{s2}/l_n . It was shown that the error which may result from this assumption was not enough to invalidate the resulting conclusions. However, as an indication of the extremes of this error, figure 23 presents the ratio of the pressure ratios across an unsteady expansion followed by a steady expansion to that across the reverse process. In each case, the initial and final Mach numbers and \bar{A} of the nozzle are identical. From this figure, it can be concluded that the assumption for preliminary information is justified.

(5) It has been assumed that the flow in all nozzles is one dimensional. This assumption allows analytical solutions throughout the nozzle and is reasonable as long as it is not used to describe expansions through large \bar{A} in extremely short nozzle lengths. When such a situation exists, errors in flow properties may become significant. Account must also be taken in such cases, of the shock waves necessary to turn the flow through the angle that will be formed at the junction of the nozzles and the acceleration chamber. These standing waves may interfere with the test flow to the extent that it becomes useless. The configuration producing such a flow would be of no value.

(6) It has been assumed that the unsteady expansion fan, after passing through the nozzle, may be treated as a centered expansion. It is clear from the general unsteady characteristic equations (ref. 4) that this is an approximation. It is believed, however, that because of the extent of the expansion fan downstream of the nozzle, and with the determination of the "virtual center" of expansion, the effects of this approximation can be minimized and reasonable results obtained.

Configuration I

From the foregoing analysis, it has been determined that for $\bar{A} \geq 10$ and $(a_4/a_5)_0 \cong (a_4/a_5)_I$, the perfectly expanded configuration suffers severe penalties in driver pressure requirements when compared to the basic expansion tube.

Figure 5 indicates that the driver sound speed requirements for a perfect expansion are modest – that is, $(a_4/a_5)_{\bar{A}} \leq 11.0$ for $\bar{A} \geq 10$, $M_5 \leq 50$. These requirements are well within the realm of present-day technology and pose no problems.

For configurations I and II, the intermediate-chamber parameter, $\frac{p_1(a_5)^2}{p_5(a_1)^2}$ for arbitrary values of \bar{A} , is represented in figure 13 by the curve for $\bar{A} = 1.0$. The ratio p_1/p_5 , which for this case is identical to that for the expansion tube, increases with M_5 and decreases with a_5/a_1 .

The acceleration-chamber parameter $\frac{p_5(a_{10})^2}{p_{10}(a_5)^2}$ for configurations I, II, and III is shown in figure 14 and is independent of \bar{A} . The pressure ratio p_5/p_{10} increases with M_5 , decreases with a_{10}/a_5 , and, being independent of \bar{A} , is identical to the same parameter computed for the expansion tube.

The required driver length for most efficient operation of configuration I is presented in figure 15 and is compared at the same values of a_4 with its counterpart for constant area tube operation, this being denoted by the curve labeled "Expansion tube." The comparison reveals that even for relatively long nozzles, that is, $l_n/l_{s1} \approx 0(1)$, advantages may be realized when $\bar{A} > 40$.

The acceleration-chamber length required for maximum test time is shown for configurations I and II as well as for the expansion tube in figure 16. As previously noted, this length is independent of \bar{A} and is, for reasonable values of l_{s1} , quite large. So large in fact is l_{s2} , that it must necessarily be made shorter than the length yielding maximum test time even though use is made of only a fraction of the processed gas. Economic as well as viscous interaction problems force this decision.

Configuration II

The driver pressure parameter Φ_{II} is shown in figure 10. From this figure, it is apparent that this configuration requires a driven pressure substantially higher than that necessary for the expansion tube. Comparisons are made at equal driver sound speeds. There are, however, significant reductions in p_4 for configuration II when compared with those for configuration I. These gains come at the expense of driver sound speed a_4 being higher for configuration II.

Limitations on the operating range for configuration II are, at the higher end, values of M_5 at which a perfect expansion occurs and at the lower end, values of M_5 such that $M_e \geq M_{eS}$. These and the possibility of a boundary-layer-separation limitation have been discussed.

The comparison of the driver length of configuration II with those of configuration I and the expansion tube is made clear by a consideration of figures 15 and 17. The driver for configuration II is considerably longer than that for configuration I and slightly shorter than that for the expansion tube. This difference is a result of the higher sound speeds required for configuration II and the differing expansion processes in the facilities.

Intermediate- and acceleration-chamber pressures as well as acceleration-chamber length were included in the discussion of configuration I.

Configuration III

The driver parameter Φ_{III} is shown in figure 12. At the lower values of M_5 , configuration III permits some reduction of p_4 when compared with configurations I and II. This, however, is true primarily for higher values of a_4 . For low driver sound speeds, the limiting state for the expanding driver gas is reached at a lower value of M_5 than that for the expansion tube, resulting in higher driver pressures at moderate values of test-section Mach numbers. Configuration III, with regard to p_4 , is used to best advantage with large values of a_4/a_5 as seen from figure 12.

The intermediate-chamber parameter $\frac{p_1}{p_5} \left(\frac{a_5}{a_1} \right)^2$ is portrayed for configuration III by figure 13. From this figure, the value of p_1 is seen to increase with \bar{A} and M_5 and to decrease with the square of a_5/a_1 . One result of such an increase in p_1 would be the inhibition of boundary-layer effects and hence, the "leaky piston" effect reported in reference 5. A consequence of this would be that considerably more flow would be available which would be suitable for processing to test conditions.

The quantity $(l_d/l_{s1})_{III}$ is presented in figure 18 and lies within the range of 2.0 to 0.001, the low end of the range occurring at high M_5 and low $(a_4/a_5)\bar{A}$. The parameter is seen to be a strong function of M_5 and \bar{A} .

Configuration III now appears to offer the greatest possibilities as far as reducing the driver length is concerned. This conclusion, however, will bear close scrutiny since for configuration I values of $(l_d/l_{s1})_I \sim 0(10^{-2})$ can be achieved which are independent of M_5 , whereas this parameter increases rather rapidly with decreasing M_5 for configuration III. In any event, configuration III allows a driver, for all sound speeds, which is considerably shorter than that required for the expansion tube; this becomes clear from figure 18, the expansion tube curve being denoted by $\bar{A} = 1.0$. The reason for this trend

is simply that in configuration III, the reflected $u + a$ wave and the interface are allowed to intersect earlier (at the end of the driven section) than in the expansion tube. This is manifested by a shorter driver.

The critical component of configuration III then appears to be the acceleration chamber. The mass flow analysis described previously is used and the parameter $(l_{s2}/l_n)\psi$ evaluated and shown in figure 20. As pointed out, ψ is the ratio of mass unusable for testing purposes to the mass which has flowed past the test section (at the end of the expansion or accelerating section) in the interval between the arrival of the secondary interface and the last characteristic of the secondary $u - a$ expansion fan. If l_{s2}/l_n is chosen such that $\psi < 1.0$, usable flow exists at the test section. With this in mind, figure 20 makes it clear that a lengthy acceleration chamber is required if gradient free test flow is desired. Such excessive lengths may prohibit the use of configuration III.

Finally, figure 22 presents the maximum nondimensional nozzle lengths. In configurations I and II the nozzle length parameter l_n/l_{s1} played a role only to the extent that it influenced the driver length parameter l_d/l_{s1} . For configuration III, $(l_n/l_{s1})_{III}$ is considerably more important in that values of this parameter greater than those shown in figure 22 result in zero test time. Consequently, nozzles used must be shorter than indicated in figure 22 and this, since $(l_n/l_{s1})_{III}$ is rather small in most cases, results in a severe violation of the assumption of one-dimensional flow in the nozzles. The most severe consequence of this violation, not only for configuration III but also for configurations I and II, is the formation of recompression shock waves when the flow, which is not one dimensional, exiting from the nozzle is collected in a cylindrical section such as the intermediate and acceleration chambers. Any such strong shock waves will render configurations in which they occur useless.

CONCLUDING REMARKS

The configurations presented would lack feasibility in comparison with the configuration presented in NASA Technical Report R-223. This conclusion is supported primarily by a consideration of the component lengths, driver pressure, and the deviation of the flow in the nozzle from the assumed one-dimensional flow.

Configuration I is rejected due to the extreme driver pressures required (although with relatively low sound speeds).

Configuration II is rejected as a result of high driver pressure requirements coupled with the severely truncated operating regime.

Configuration III, which was believed to be most feasible, is rejected primarily because the short nozzle lengths required in order to insure the availability of testing time. Use of such short nozzles would result in strong nozzle recompression shock waves disrupting any useful test flow. It should be pointed out that similar standing waves will be present to some extent in configurations I and II possibly creating serious flow disturbances. Shortcomings of this nature are not present in the facility of NASA Technical Report R-223 since the test section is located immediately after the expanding nozzle, the test flow being utilized prior to its interaction with the recompression waves. Finally, it may be argued that configuration III requires higher driver pressures than those in the expansion tube (with the same test-section diameter) with little improvement in the viscous problems associated with the acceleration chamber.

Langley Research Center,

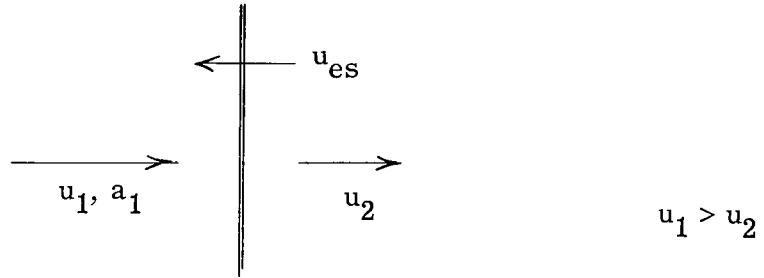
National Aeronautics and Space Administration,

Langley Station, Hampton, Va., November 4, 1965.

APPENDIX A

ADJUSTING SHOCK ANALYSIS

The following general flow situation exists (sketch A1):



Sketch A1

where u_1 , u_2 , and a_1 are known and the shock of Mach number

$$M_{es} = \frac{u_1 + u_{es}}{a_1} \quad (A1)$$

compatible with this situation is desired. From normal shock relations (ref. 6) in shock fixed coordinates the expression

$$\frac{\bar{u}_1}{\bar{u}_2} = \frac{\rho_2}{\rho_1} = \frac{(\gamma + 1)M_{es}^2}{M_{es}^2(\gamma - 1) + 2} \quad (A2)$$

is determined where

$$\left. \begin{aligned} \bar{u}_1 &= u_1 + u_{es} \\ \bar{u}_2 &= u_2 + u_{es} \end{aligned} \right\} \quad (A3)$$

Defining

$$\zeta \equiv \frac{u_1 - u_2}{a_1} \quad (A4)$$

APPENDIX A

and substituting this and equations (A3) into equation (A2) gives, after some manipulation, the desired shock Mach number as follows:

$$M_{es} = \frac{\gamma + 1}{4} \xi + \left[\left(\frac{\gamma + 1}{4} \xi \right)^2 + 1 \right]^{1/2} \quad (\text{A5})$$

APPENDIX B

NOZZLE LENGTH RATIO FOR CONFIGURATION III

The nozzle length which results in zero test time for configuration III is to be determined. Consider first sketch 3 which is a schematic representation of the situation described in this appendix. The nozzle length in this case is such that the reflected $u + a$ expansion characteristic, the last characteristic of the secondary fan, and the first usable test particle coalesce as all reach the end of l_{s2} . In order to analyze the arrangement of waves shown in sketch 3, a parameter α must be introduced in order to permit the investigation of the unsteady expansion exiting from the nozzle, with equations derived for a centered $u - a$ expansion in simple flow. This parameter represents the distance the first and last characteristics of the expansion must be extended past the nozzle exit, in the direction of decreasing x (measured from the nozzle exit), in order to intersect or reach a "virtual center of expansion." It is apparent that the center of this effective expansion is both an approximation and not at the nozzle entrance since the characteristics of the fan have been accelerated through the nozzle. Consequently, α is a working parameter, undetermined, and eliminated in the solution of the equations.

In sketch 3, the ratio of exit to entrance distances for the particle path shown is

$$\frac{\alpha + l_{s2}}{\alpha} = \frac{M_5 - 1}{M_e - 1} \left(\frac{1 + \frac{\gamma - 1}{2} M_5}{1 + \frac{\gamma - 1}{2} M_e} \right)^{\frac{2}{\gamma - 1}} \quad (B1)$$

where equation (68) has been used. For the $u + a$ wave, the ratio of exit to entrance distances is given by

$$\frac{\alpha + l_{s2}}{\alpha + x_e} = \frac{M_5 - 1}{M_e - 1} \left(\frac{1 + \frac{\gamma - 1}{2} M_5}{1 + \frac{\gamma - 1}{2} M_e} \right)^{\frac{3 - \gamma}{2(\gamma - 1)}} \quad (B2)$$

which has been derived by applying equation (36) across the unsteady fan separating regions e and 5 , multiplying both sides by $(u_5 - a_5)/(u_e - a_e)$ and substituting equation (1a) of the present paper and equation (11) of reference 7.

APPENDIX B

Two expressions for τ_e

$$\tau_e = x_e \left(\frac{1}{u_e - a_e} - \frac{1}{u_e + a_e} \right) \quad (B3)$$

$$\tau_e = \tau_i + \frac{l_n}{a_e} (\xi_+ - \xi_-) \quad (B4)$$

are determined where x_e is the distance from the beginning of l_{s2} (or end of the nozzle) to the point at which the $u + a$ characteristic enters the fan and

$$\tau_i = \frac{l_{s1}}{a_2} \sqrt{\frac{\gamma(\gamma-1)}{2} \frac{\gamma-1}{\gamma+1}} \quad (B5)$$

The accelerating chamber length l_{s2} is given by

$$l_{s2} = \left(\frac{l_{s2}}{l_n} \tilde{\psi} \right) l_n \quad (B6)$$

the tilde notation indicating a value of ψ equal to unity.

If the variables in equations (B1) to (B6) are eliminated and equation (1b) is used across regions 2 and e, the following expression for $(l_n/l_{s1})_{III}$ results:

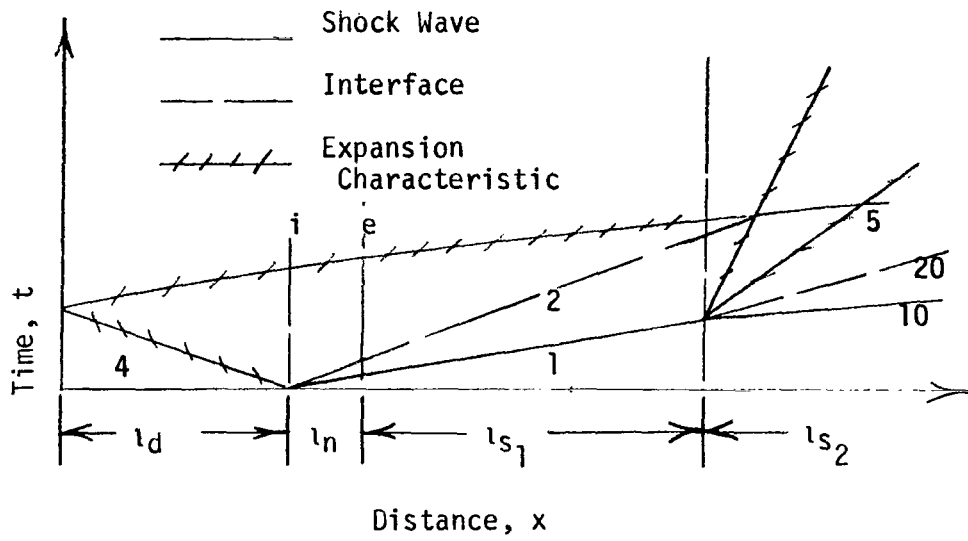
$$\left(\frac{l_n}{l_{s1}} \right)_{III} = \frac{\left[\frac{(\gamma-1)(\gamma+1)}{2 \left(1 + \frac{\gamma-1}{2} M_e^2 \right)} \right]^{1/2} \left(\frac{\gamma-1}{\gamma+1} \right) \frac{1}{2} (M_e + 1)(M_e - 1)}{\frac{l_{s2}}{l_n} \tilde{\psi} \left[\frac{\frac{M_5 - 1}{M_e - 1} \left(\frac{1 + \frac{\gamma-1}{2} M_5}{1 + \frac{\gamma-1}{2} M_e} \right)^{\frac{\gamma+1}{2(\gamma-1)}} - 1}{\frac{M_5 - 1}{M_e - 1} \left(\frac{1 + \frac{\gamma-1}{2} M_5}{1 + \frac{\gamma-1}{2} M_e} \right)^{\frac{2}{\gamma-1}} - 1} \right]} + \frac{1}{2} (\xi_- - \xi_+) (M_e^2 - 1)} \quad (B7)$$

APPENDIX B

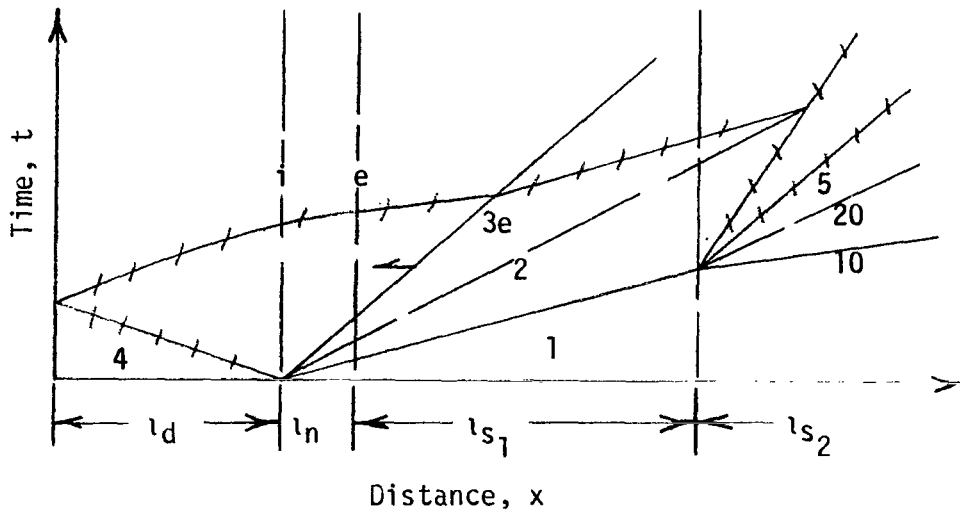
Equation (B7) is a function of A and M_5 and gives the nozzle length for which zero test time exists at the end of l_{s2} . Values of $(l_n/l_{s1})_{III}$ smaller than those given by equation (B7) produce usable test time.

REFERENCES

1. Trimpi, Robert L.: A Preliminary Theoretical Study of the Expansion Tube, a New Device for Producing High-Enthalpy Short-Duration Hypersonic Gas Flows. NASA TR R-133, 1962.
2. Trimpi, Robert L.; and Callis, Linwood B.: A Perfect-Gas Analysis of the Expansion Tunnel, a Modification to the Expansion Tube. NASA TR R-223, 1965.
3. Lukasiewicz, J.: Shock Tube Theory and Applications. Rept. 15, Natl. Aeron. Estab. Canada, 1952.
4. Emmons, Howard W., ed.: Fundamentals of Gas Dynamics. Vol. III of High Speed Aerodynamics and Jet Propulsion. Princeton Univ. Press, c.1958.
5. Duff, Russell E.: Shock-Tube Performance at Low Initial Pressure. Phys. Fluids, vol. 2, no. 2, Mar.-Apr. 1959, pp. 207-216.
6. Ames Research Staff: Equations, Tables, and Charts for Compressible Flow. NACA Rept. 1135, 1953. (Supersedes NACA TN 1428.)
7. Grose, William L.; and Trimpi, Robert L.: Charts for the Analysis of Isentropic One-Dimensional Unsteady Expansions in Equilibrium Real Air With Particular Reference to Shock-Initiated Flows. NASA TR R-167, 1963.

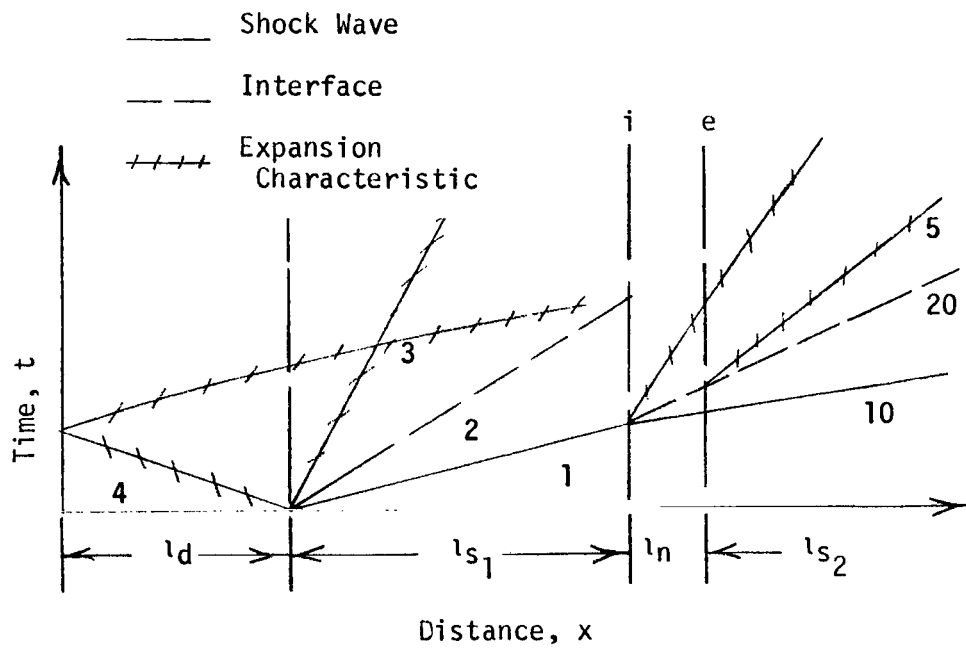


(a) Configuration I.



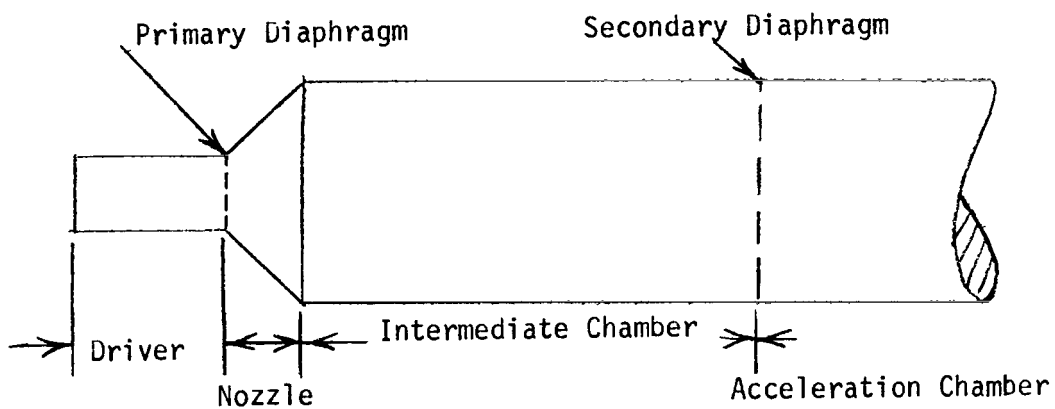
(b) Configuration II.

Figure 1.- Wave schematic.

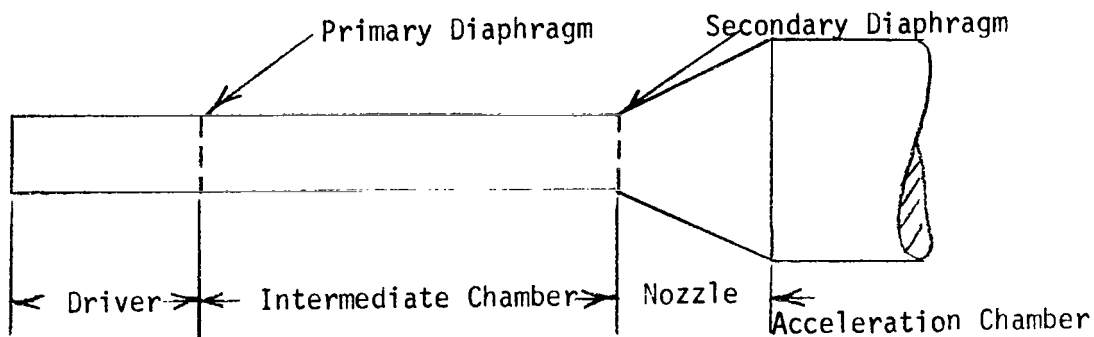


(c) Configuration III.

Figure 1.- Concluded.



(a) Configurations I and II.



(b) Configuration III.

Figure 2.- Physical schematic.

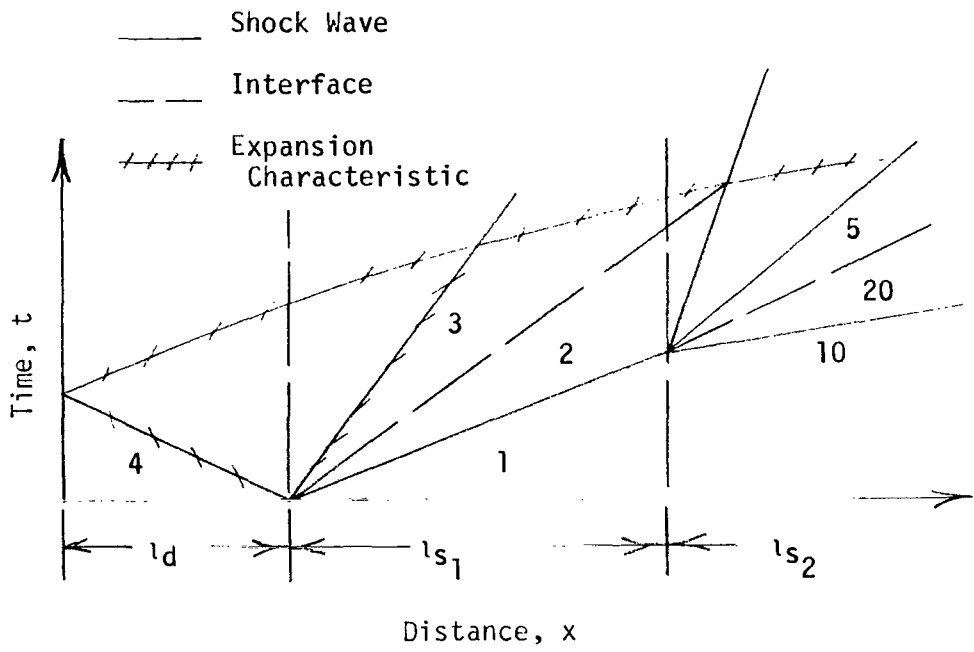


Figure 3.- Wave schematic for basic expansion tube.

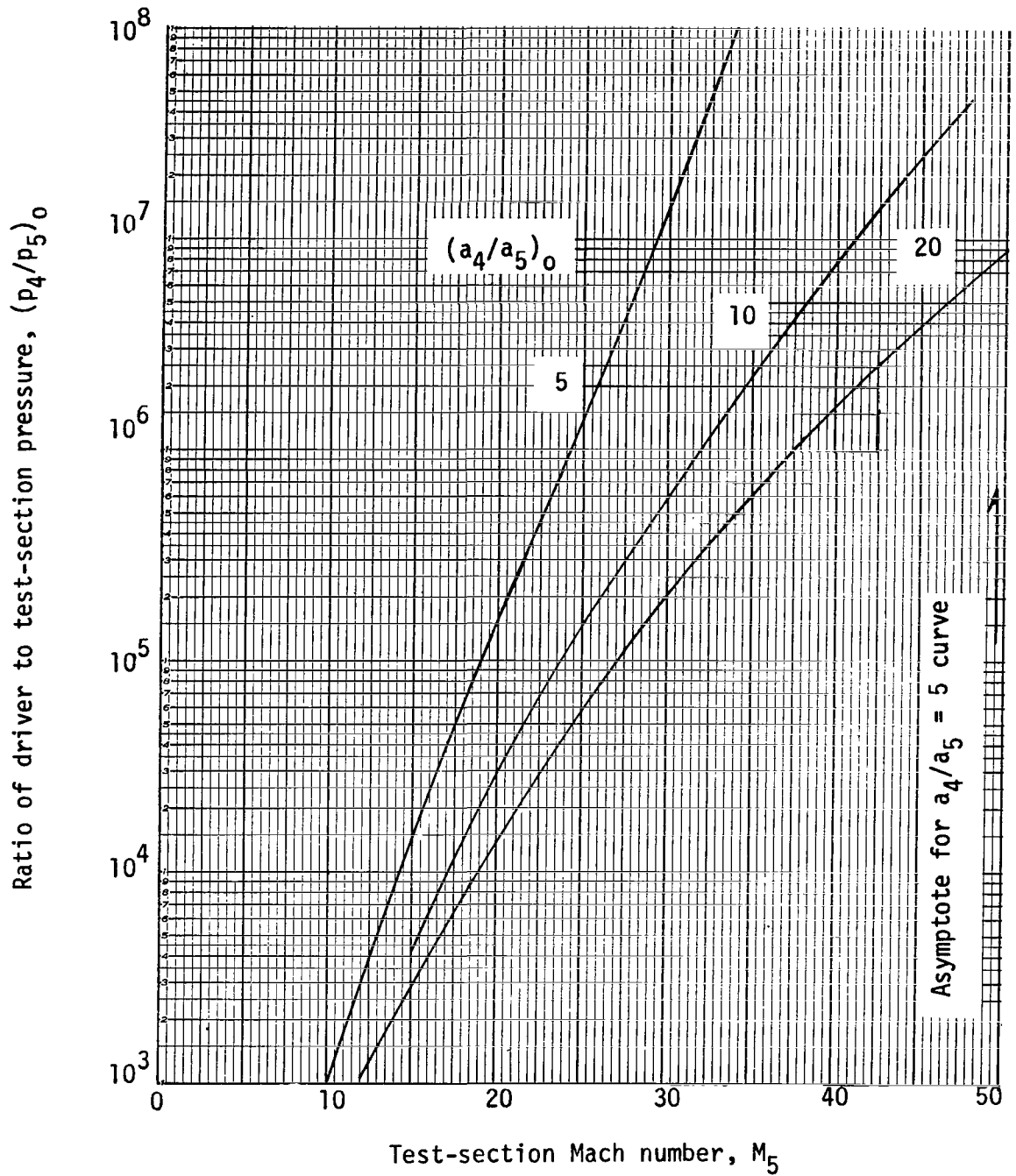


Figure 4.- Variation of driver pressure ratio with test-section Mach number for basic expansion tube.

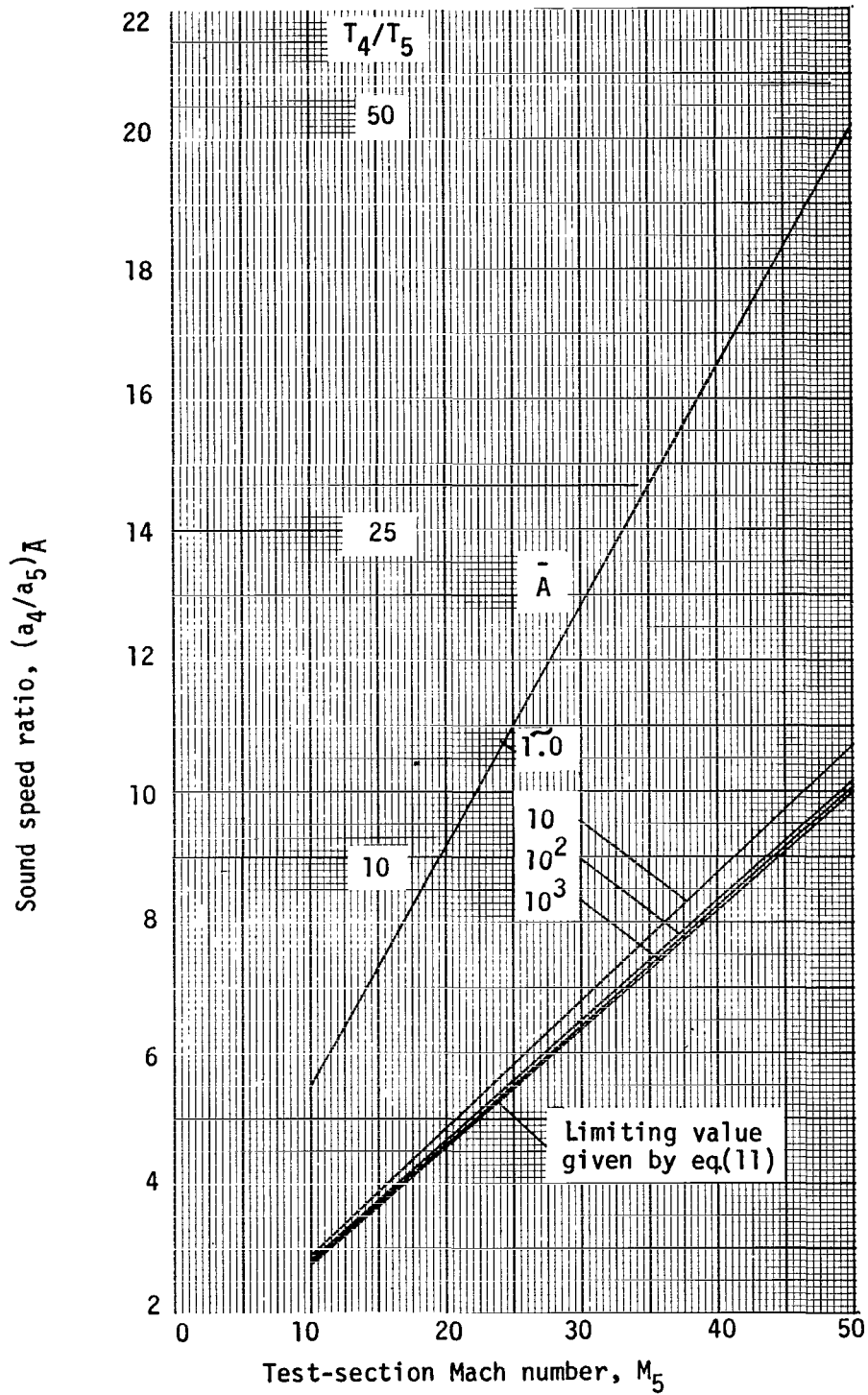


Figure 5.- Ratio of required driver to test-section sound speed for configuration I.

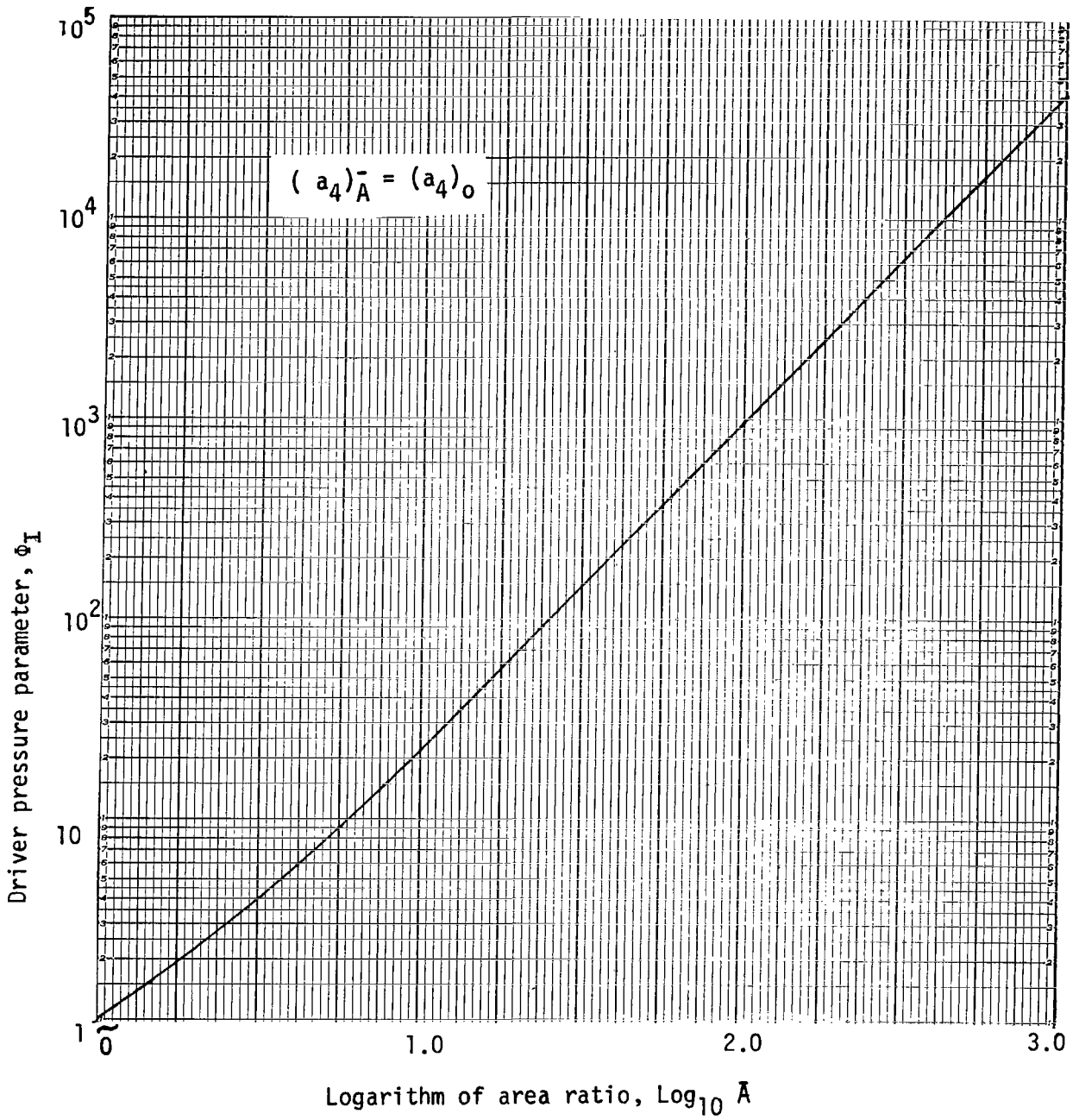


Figure 6.- Variation of driver pressure parameter for configuration I.

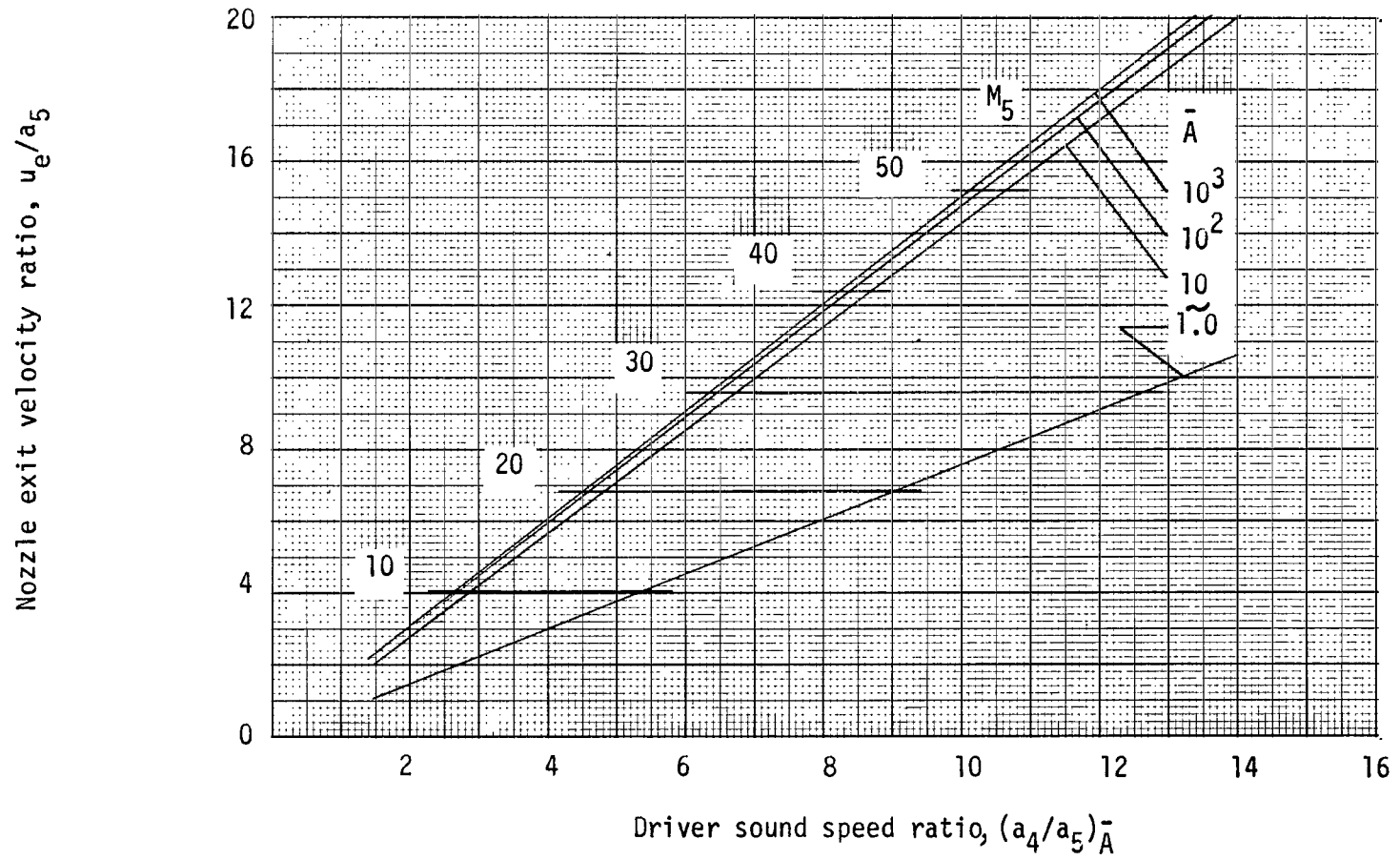


Figure 7.- Ratio of nozzle exit velocity to test-section sound speed.

Logarithm of driver pressure ratio, $\text{Log}_{10} (p_4/p_5) \bar{A}$

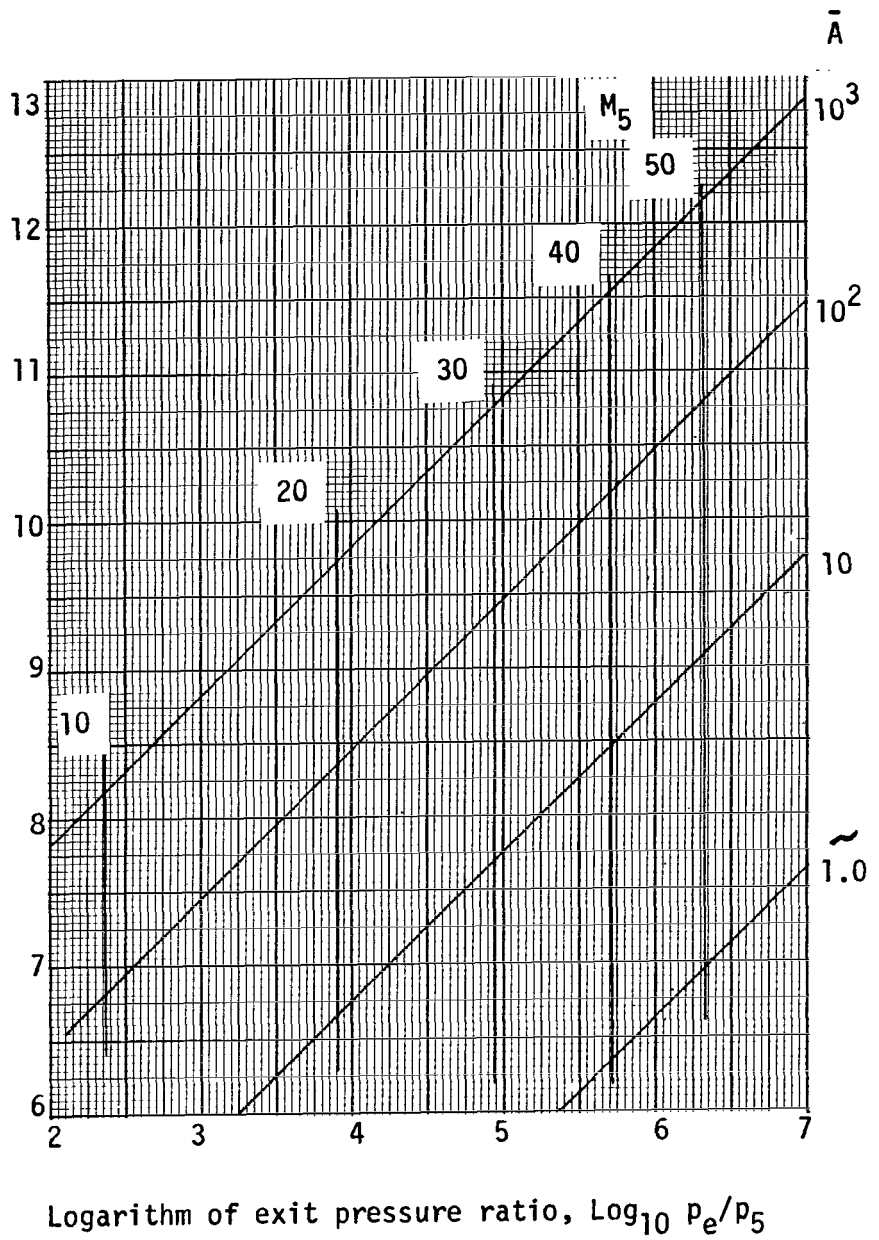


Figure 8.- Logarithm of ratio of nozzle exit to test-section pressures for configurations I and II.

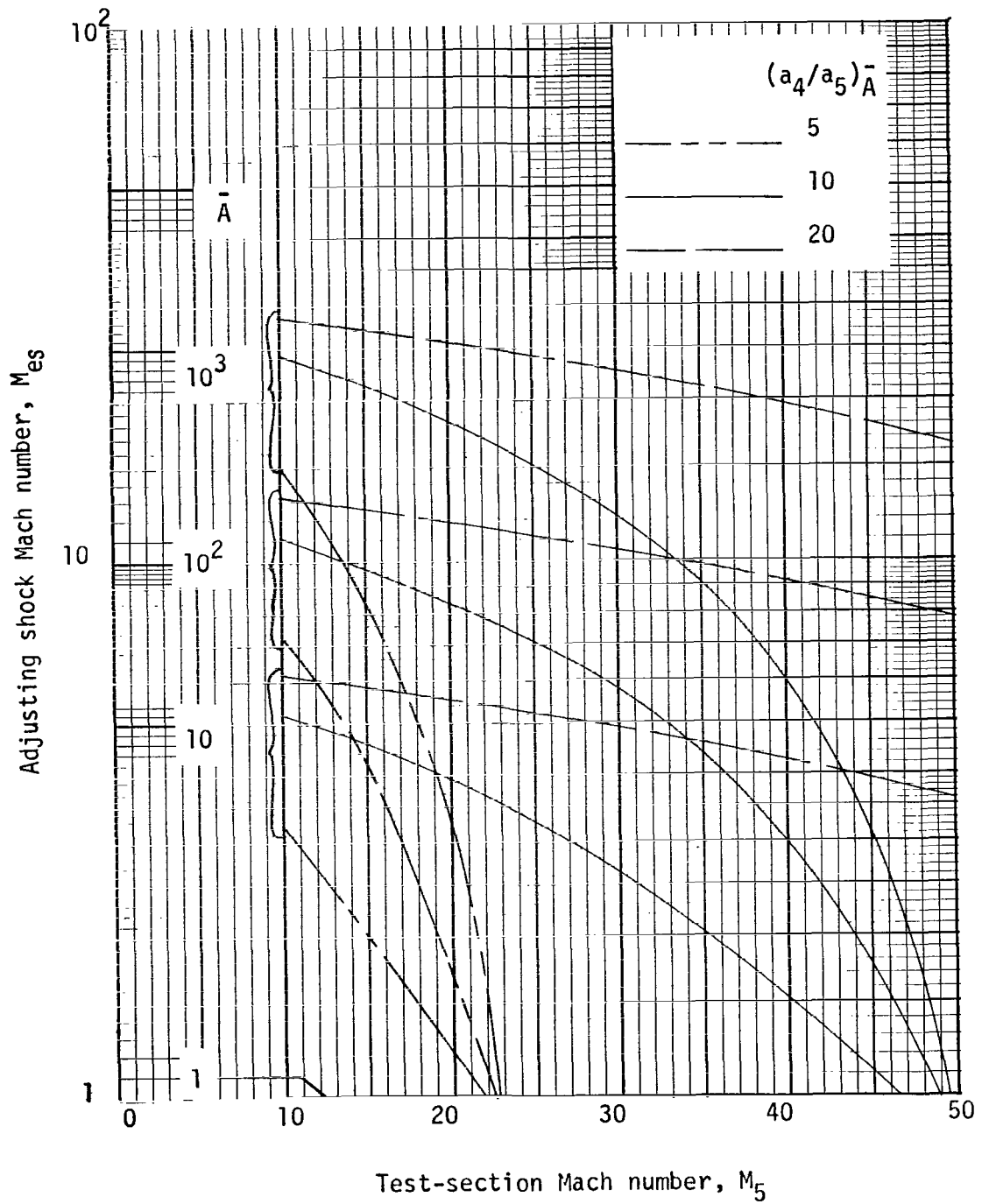
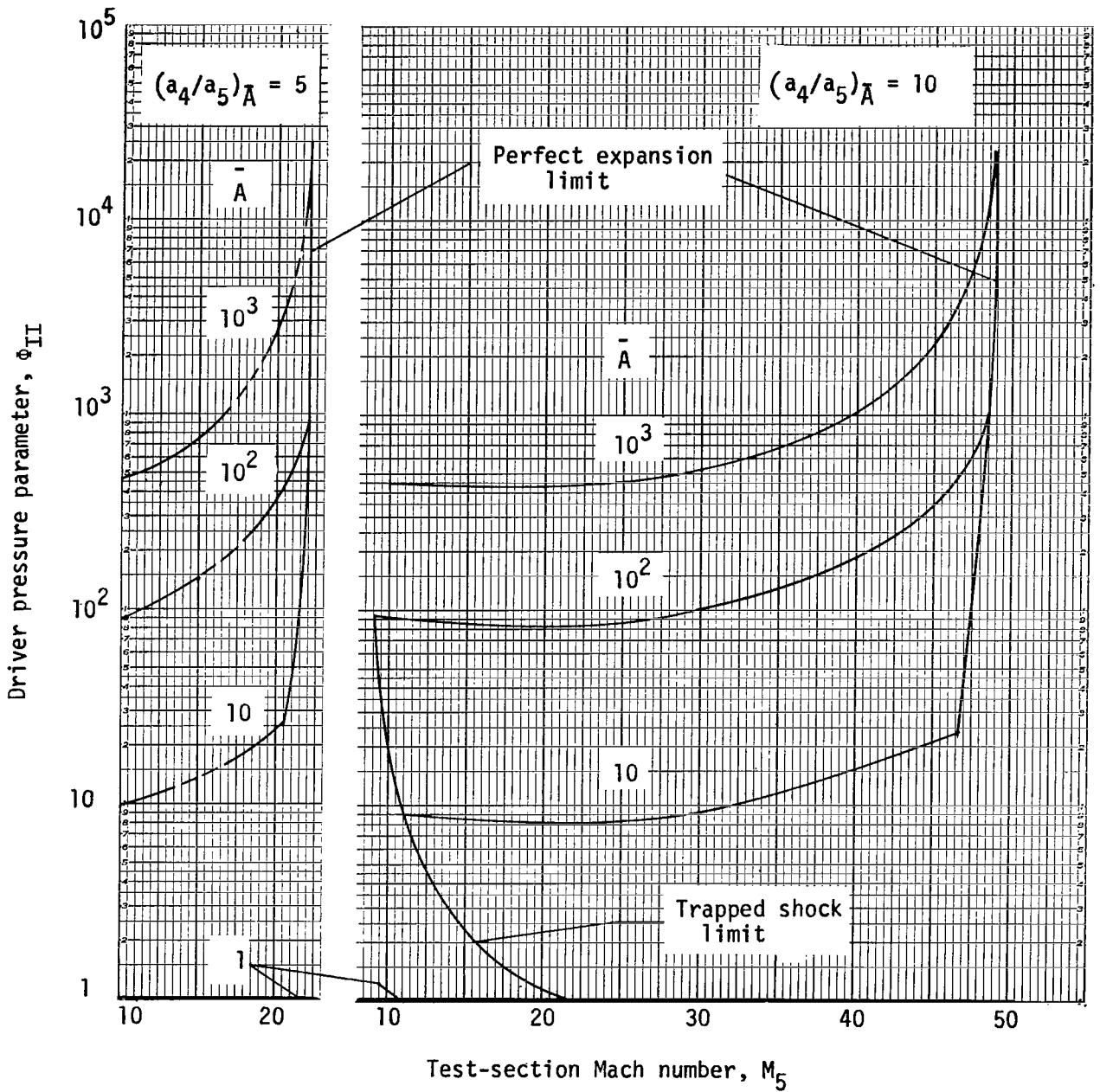
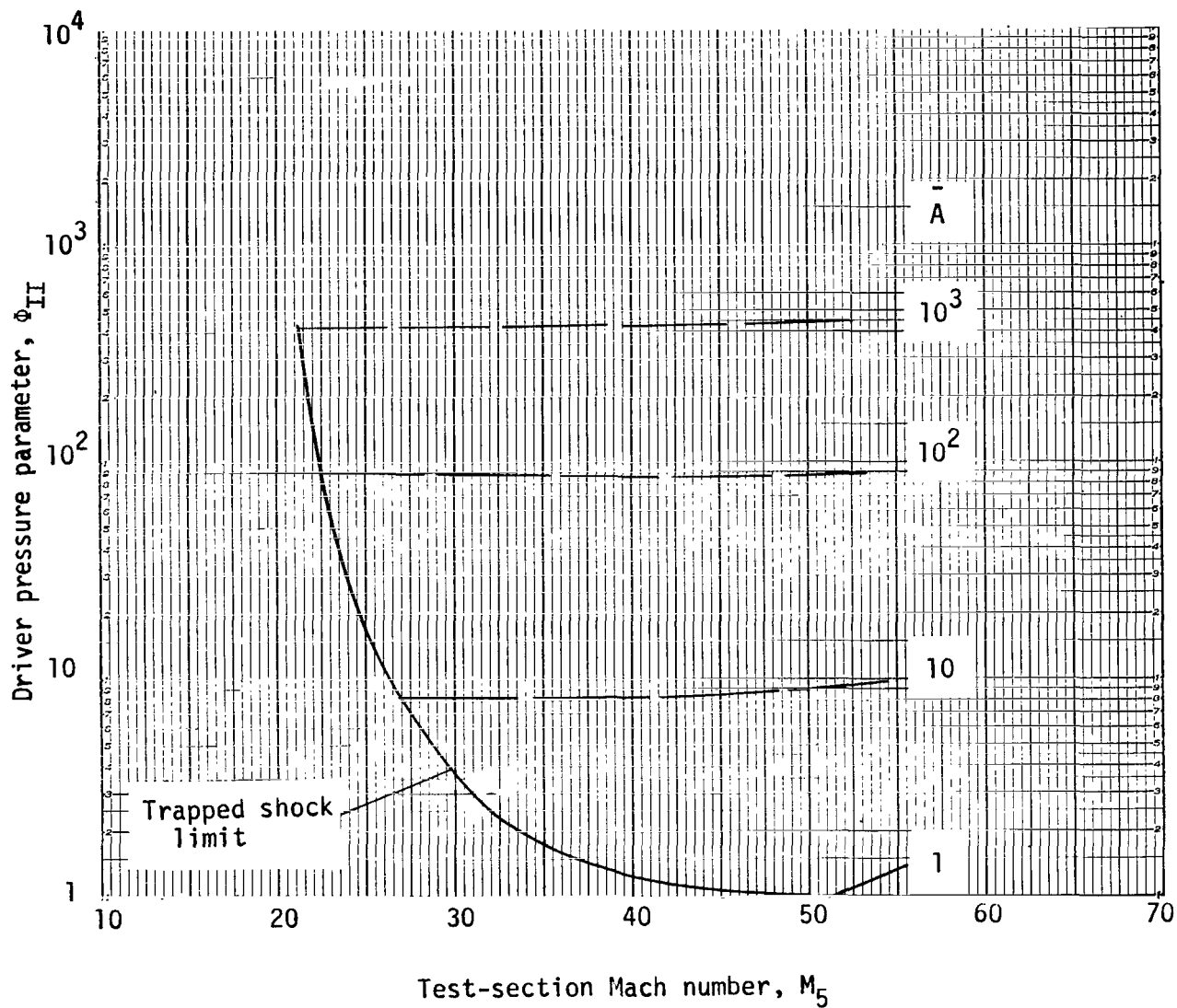


Figure 9.- Adjusting shock Mach number required for configuration II.



(a) $(a_4/a_5)_{\bar{A}} = 5$ and 10.

Figure 10.- Variation of driver pressure parameter for configuration II.



(b) $(a_4/a_5)_A = 20.$

Figure 10.- Concluded.

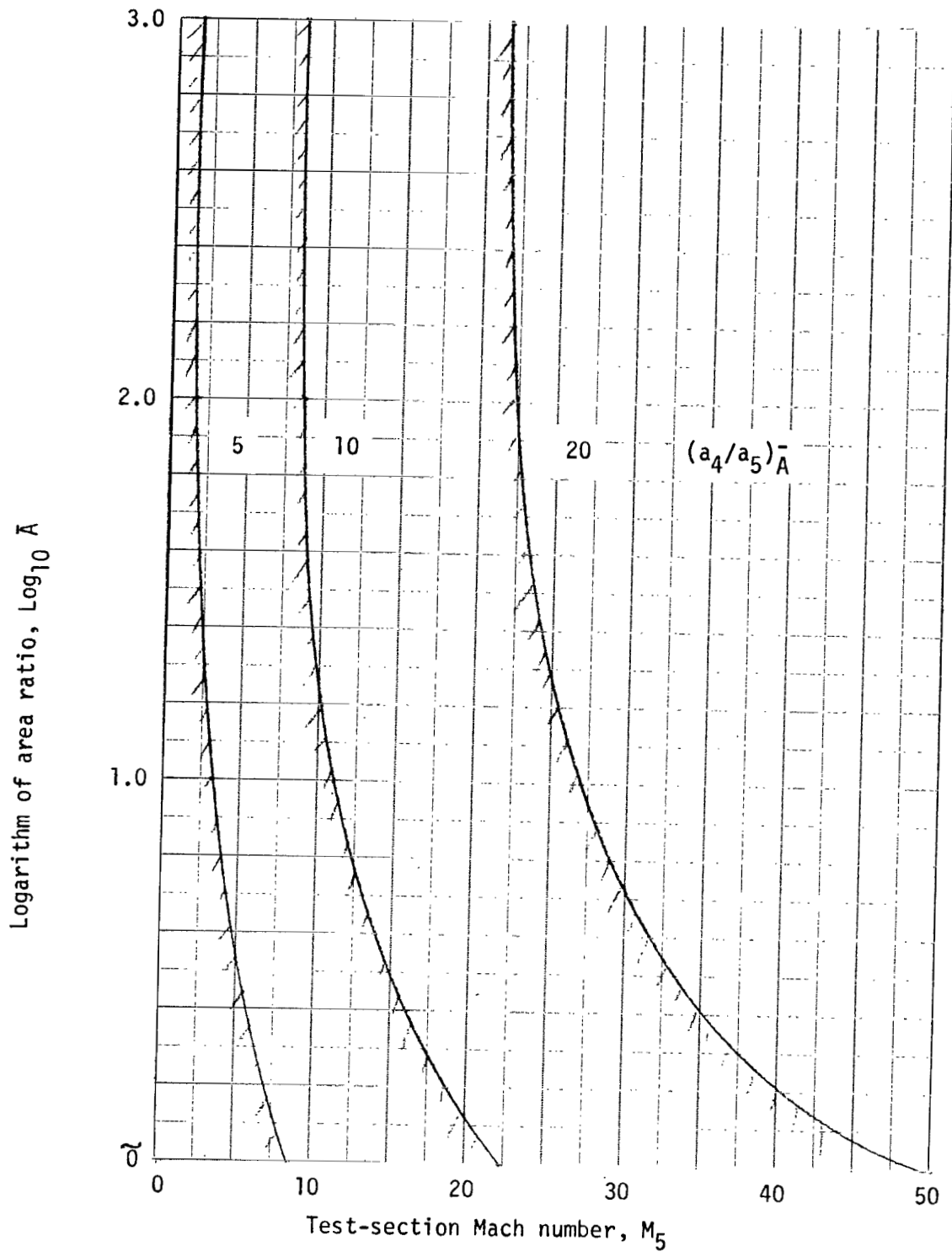
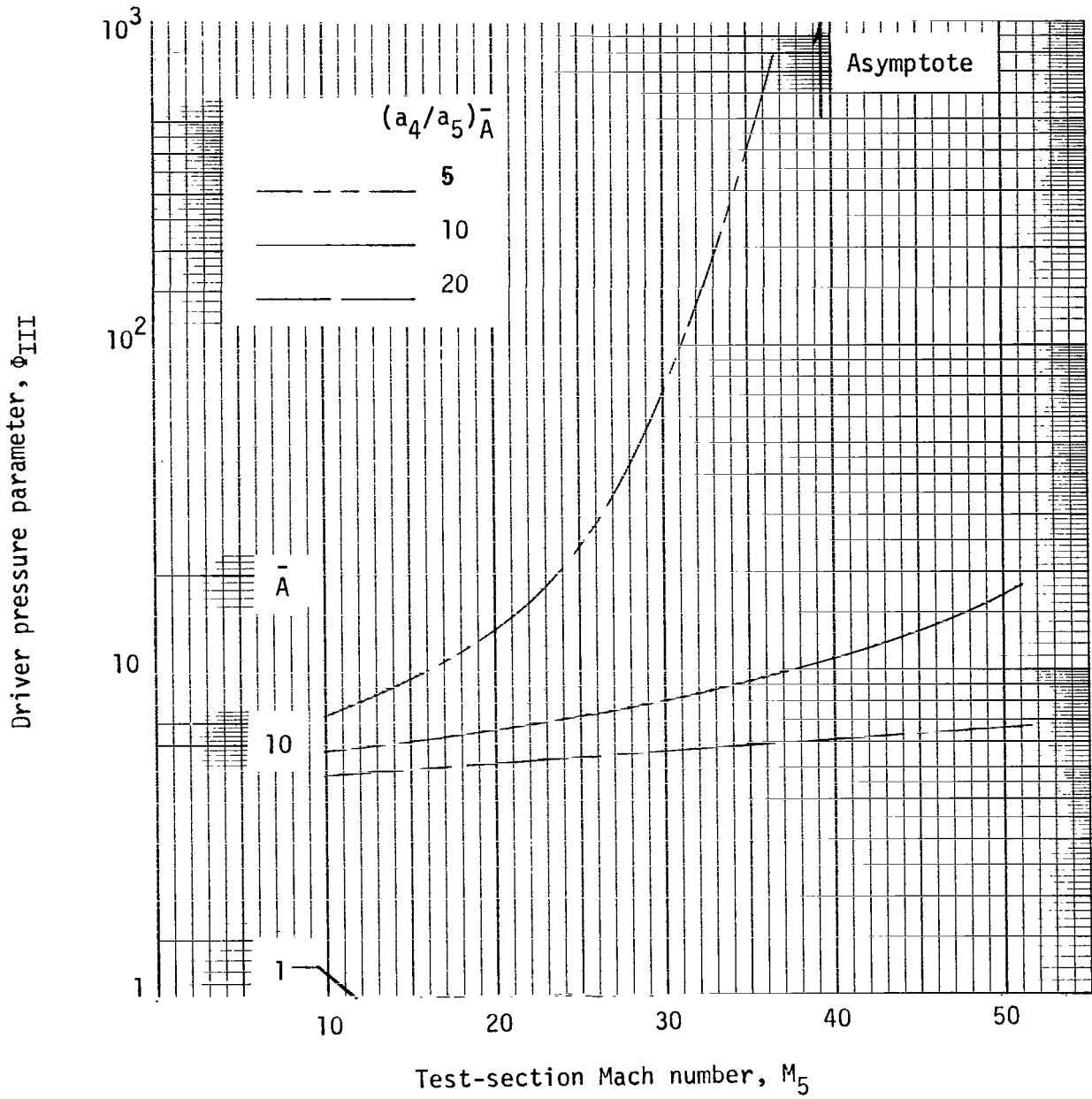
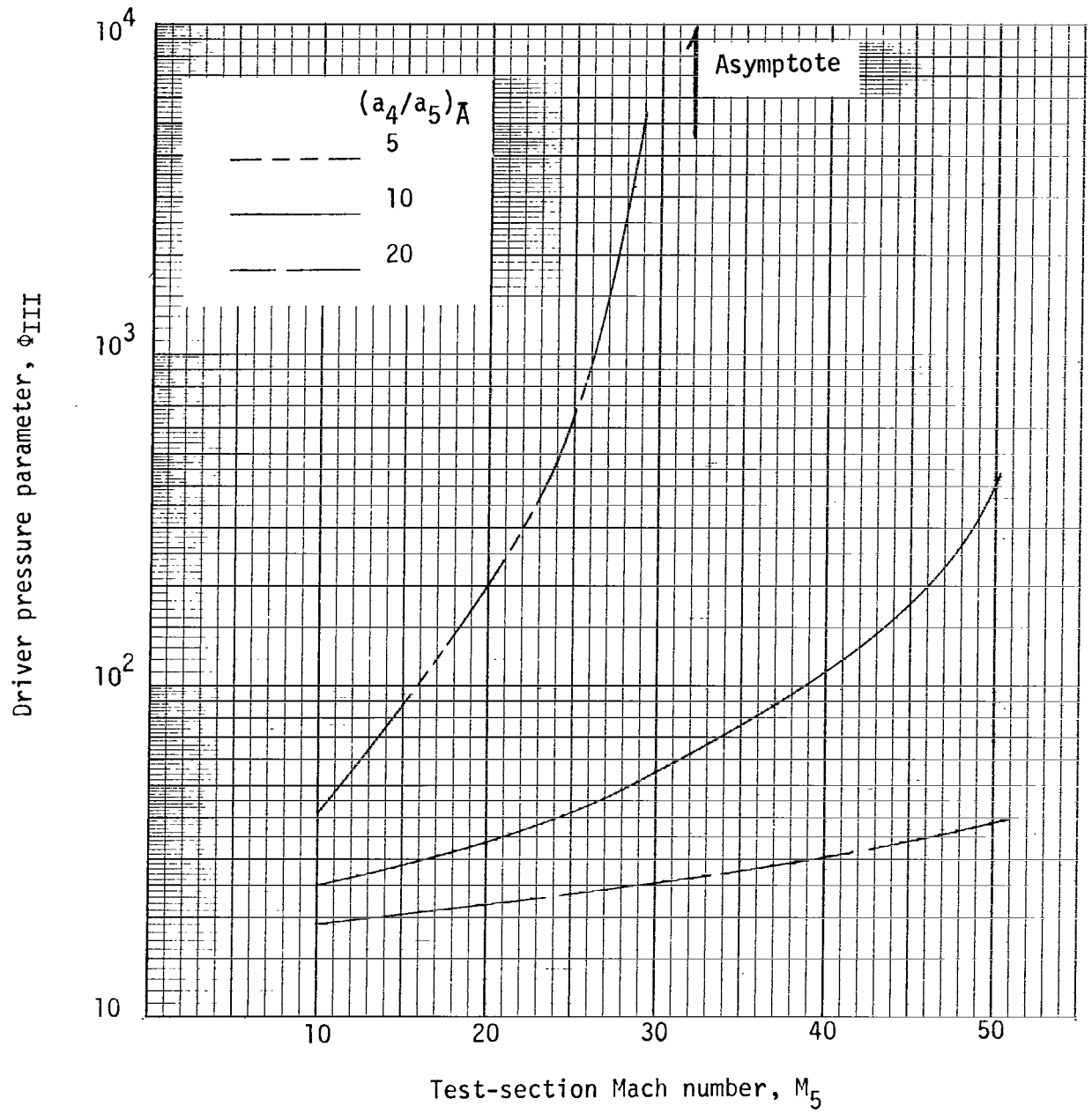


Figure 11.- Limiting M_5 to avoid trapped shock for configuration II.



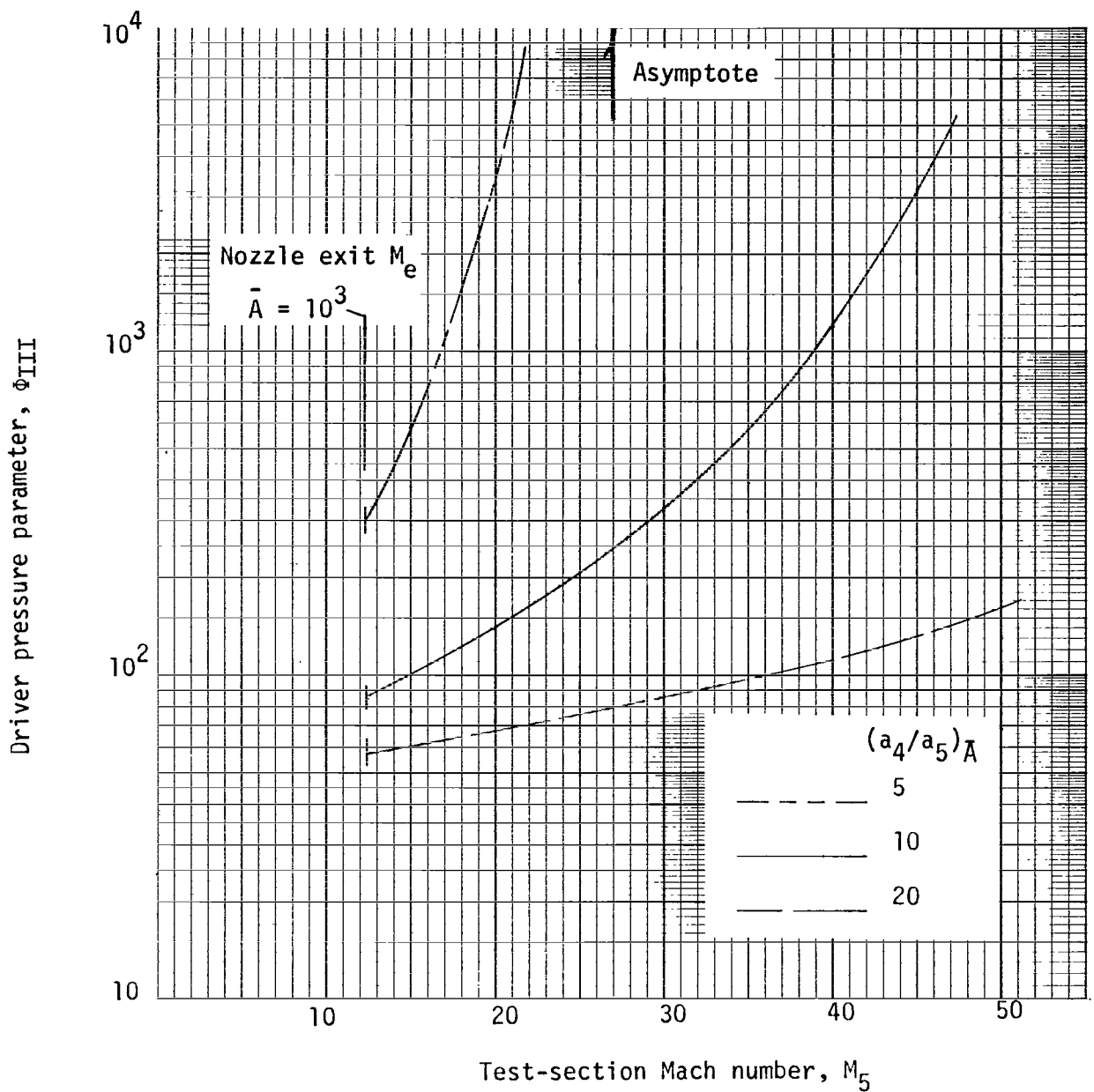
(a) $\bar{A} = 1$ and 10.

Figure 12.- Variation of driver pressure parameter for configuration III.



(b) $\bar{A} = 10^2$.

Figure 12.- Continued.



(c) $\bar{A} = 10^3$.

Figure 12.- Concluded.

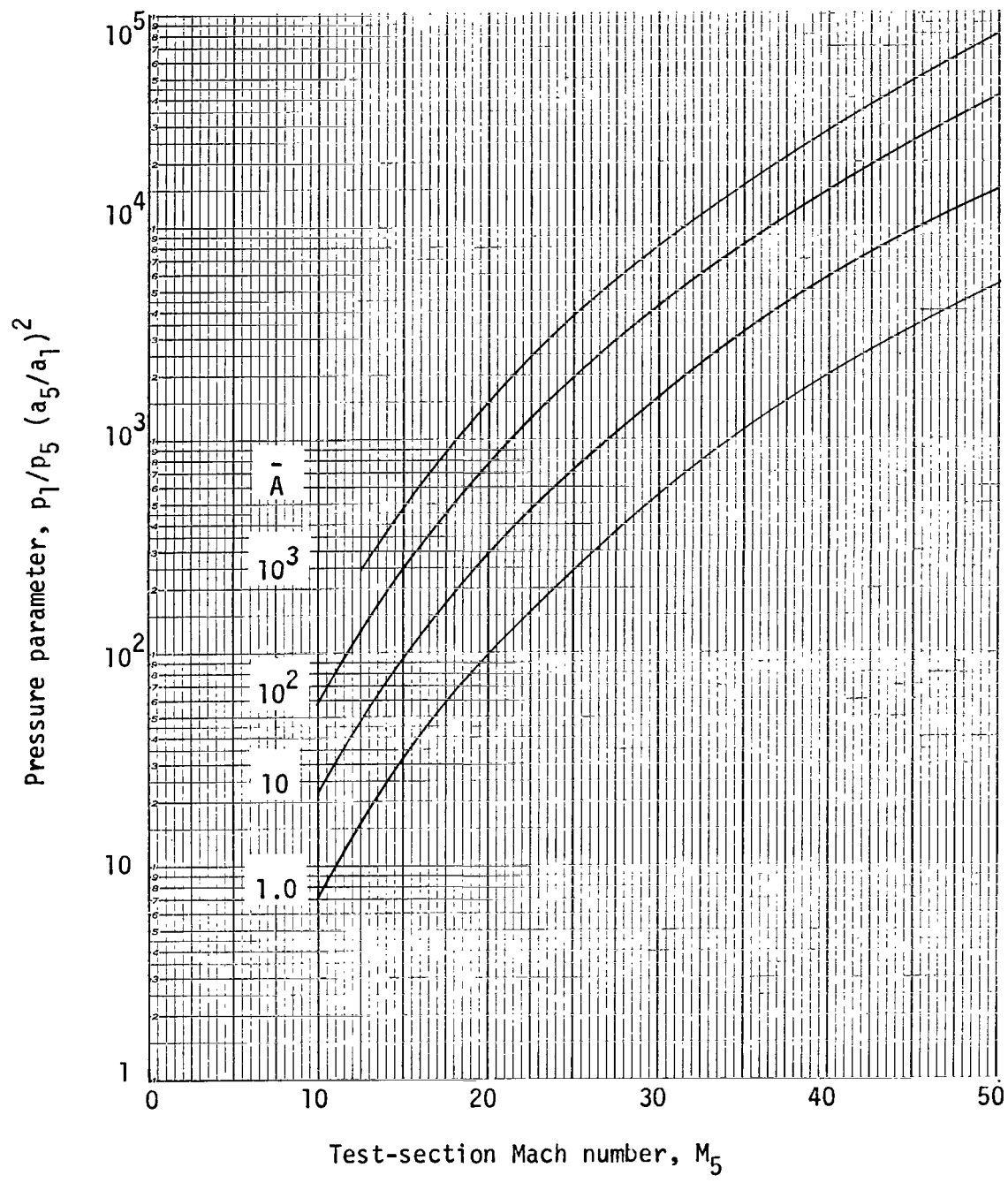


Figure 13.- Variation of intermediate-chamber pressure parameter for configuration III. Curve for $\bar{A} = 1.0$ is also valid for configurations I and II for all \bar{A} .

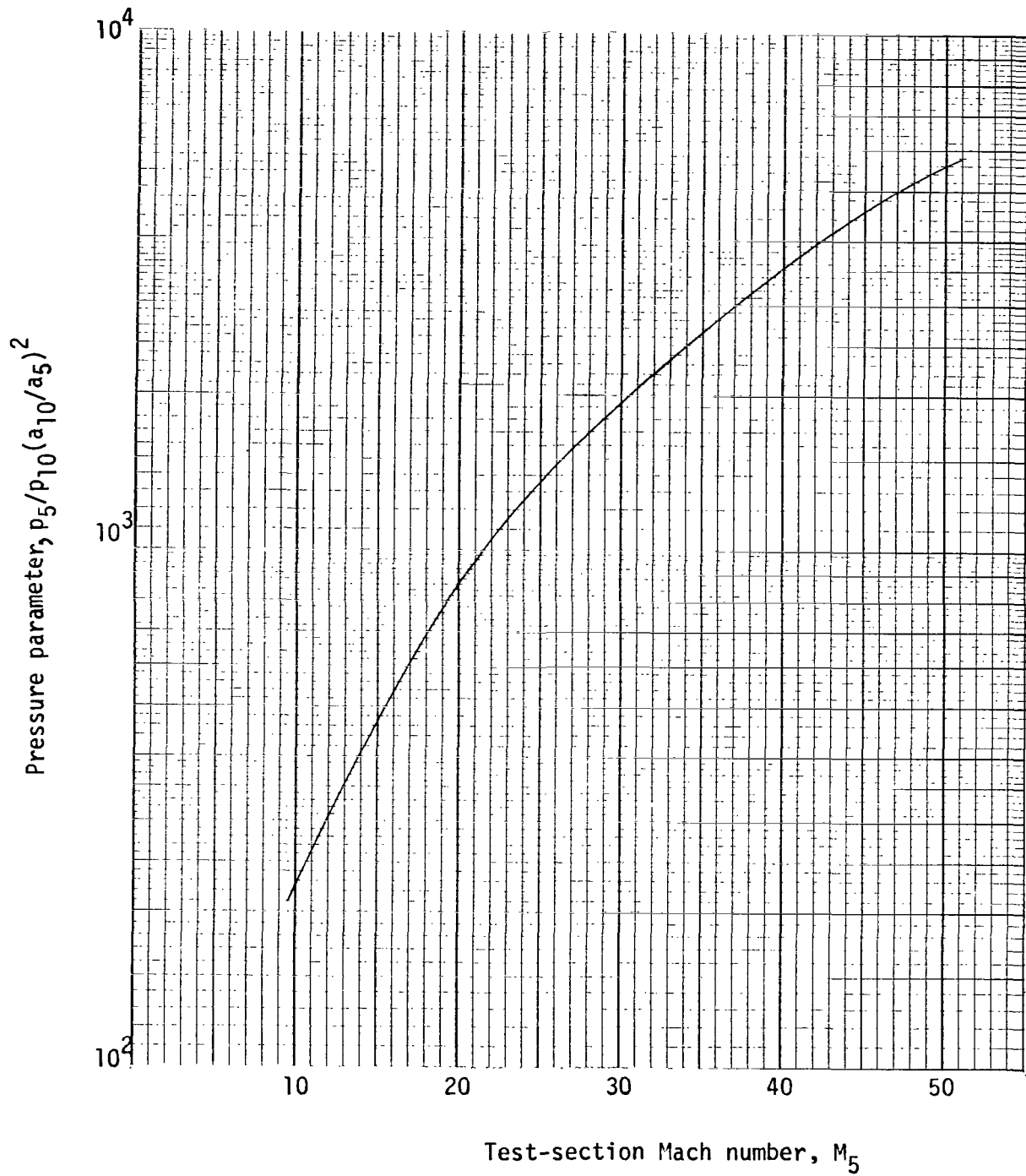


Figure 14.- Variation of acceleration-chamber pressure parameter for all configurations.

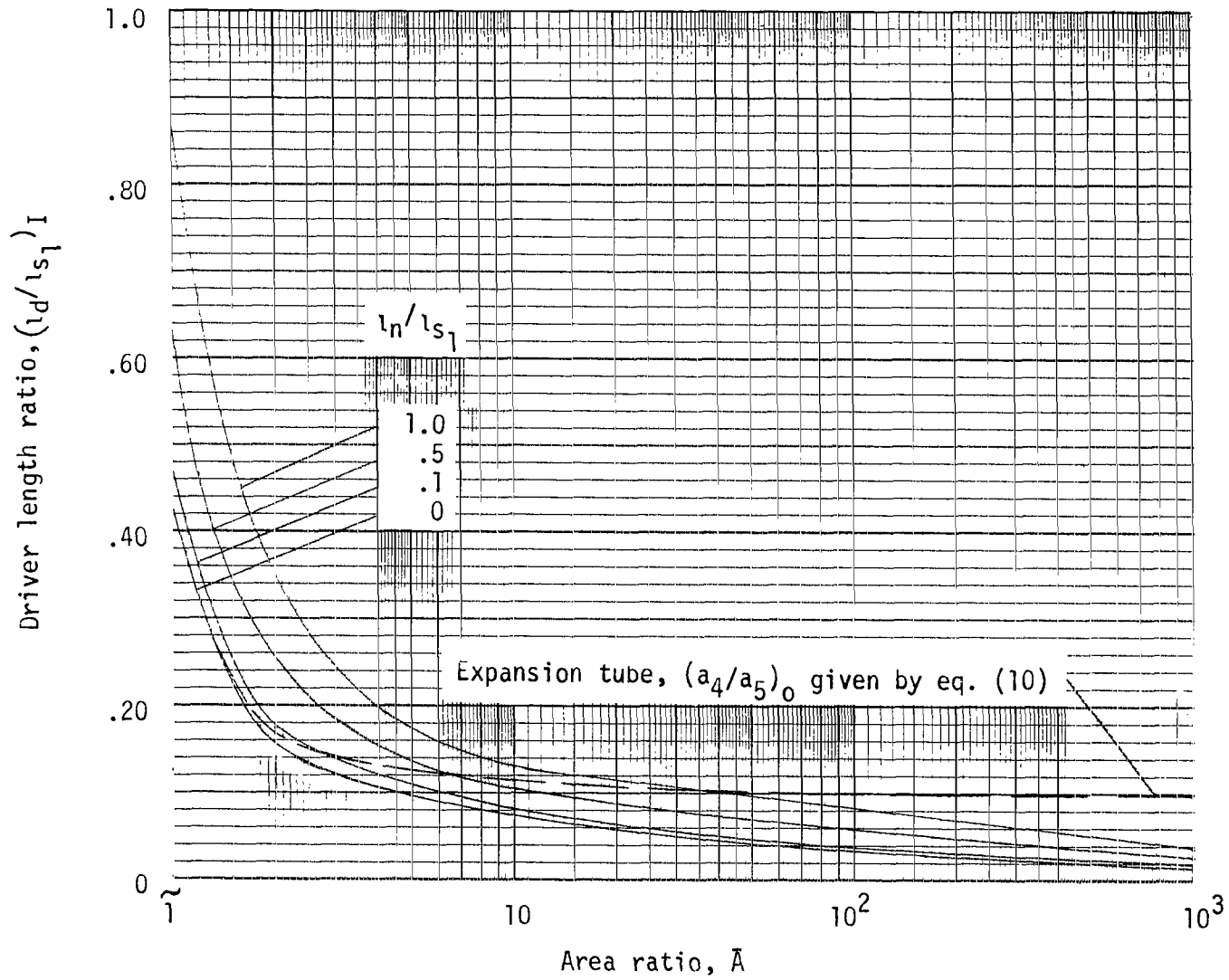


Figure 15.- Driver to intermediate-chamber length ratio for configuration I.

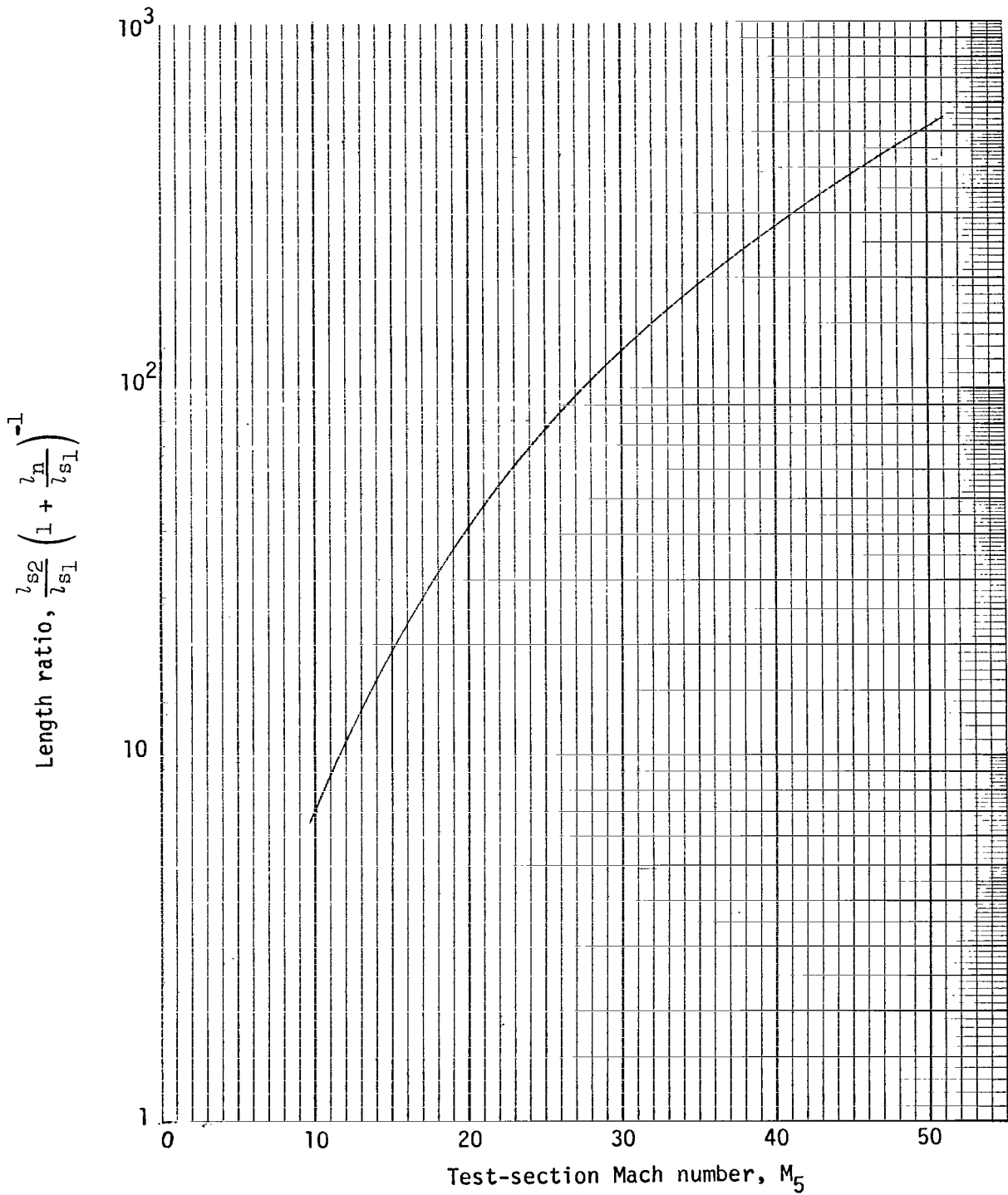
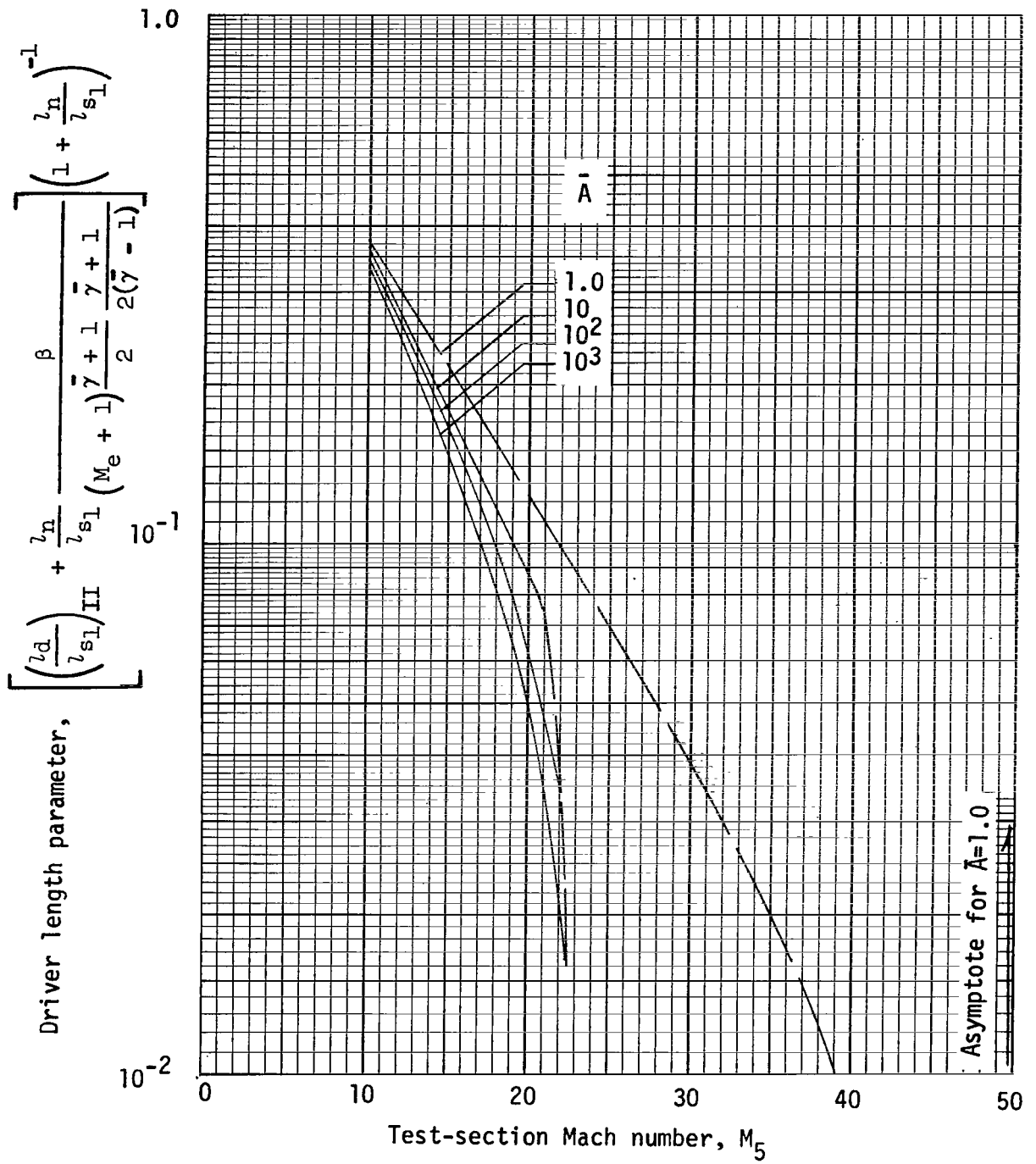
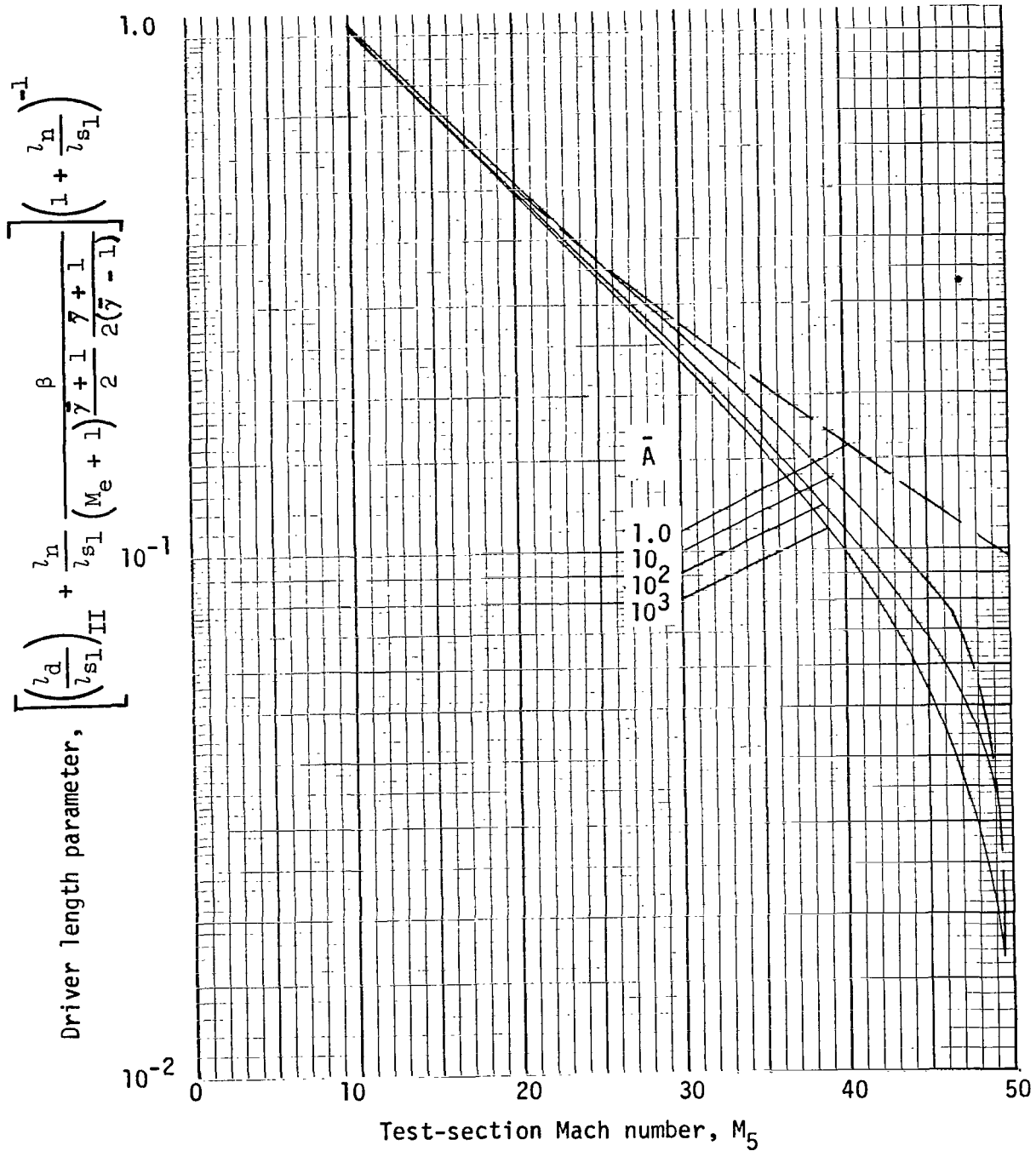


Figure 16.- Ratio of acceleration to intermediate chamber length for configurations I and II.



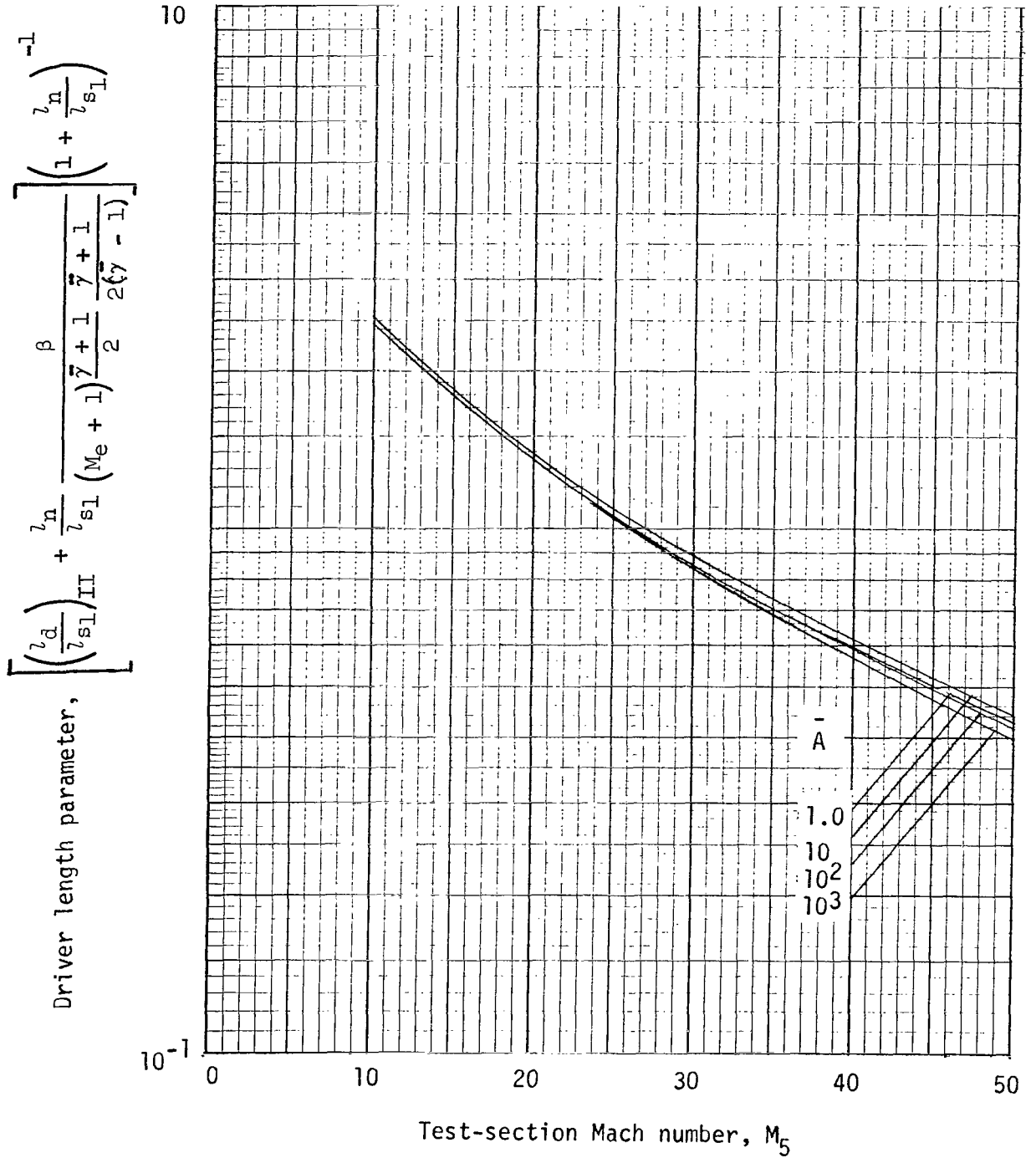
(a) $(a_4/a_5)_{\bar{A}} = 5.0$.

Figure 17.- Variation of driver-section length parameter for configuration II.



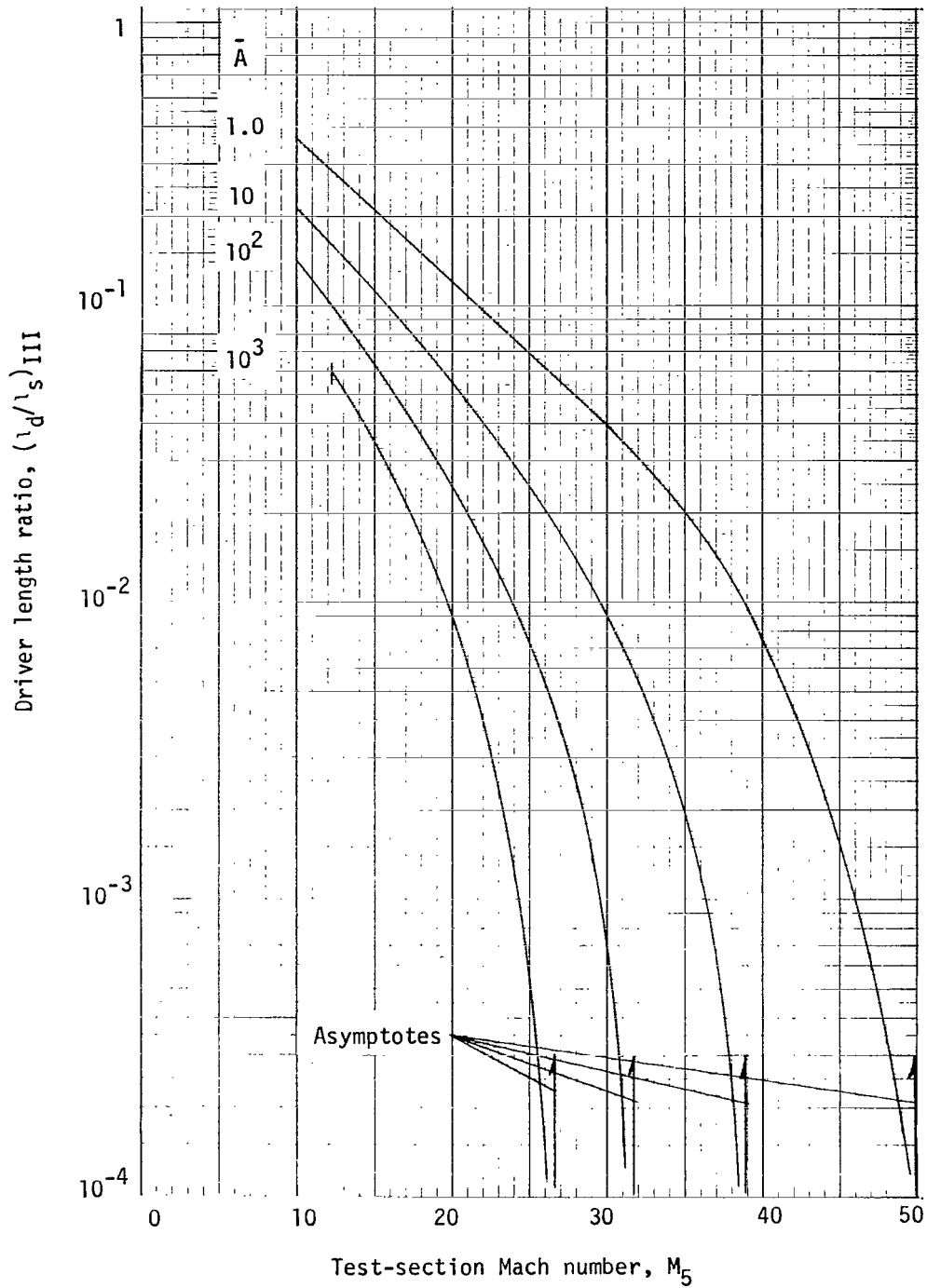
(b) $(a_4/a_5)_{\bar{A}} = 10.0$.

Figure 17.- Continued.



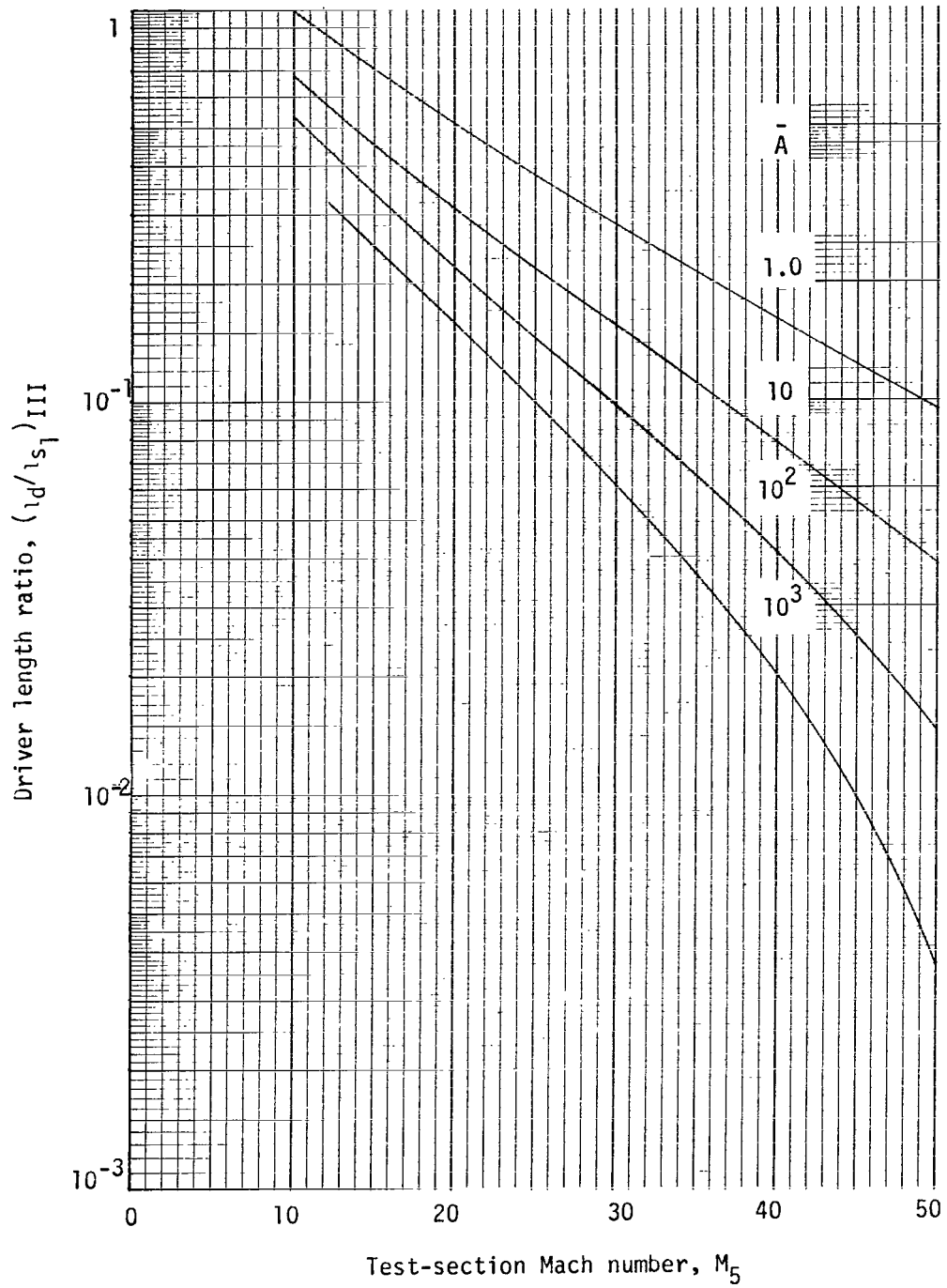
(c) $(a_4/\beta_5)_A = 20.0$.

Figure 17.- Concluded.



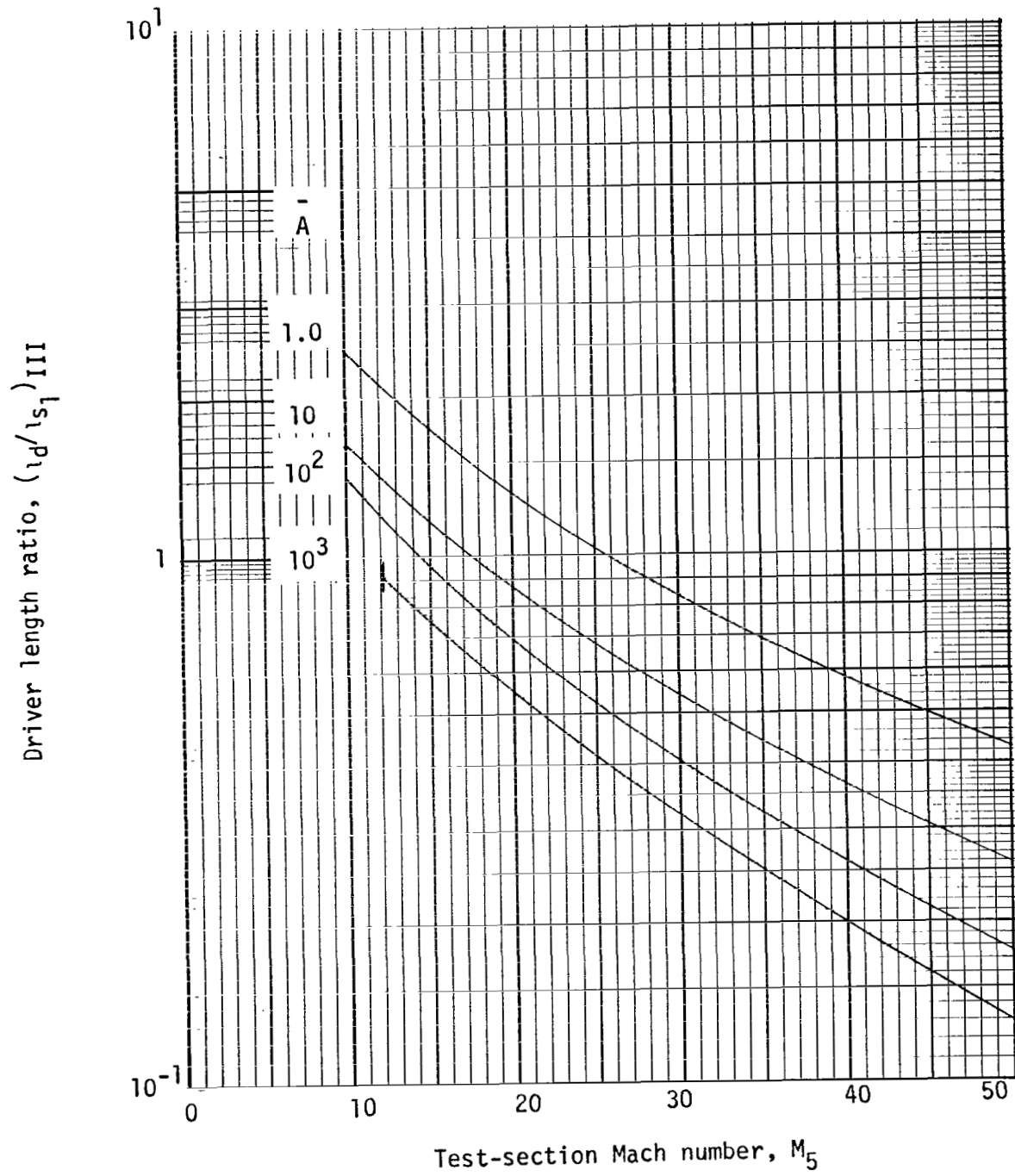
(a) $(a_4/a_5)_{\bar{A}} = 5.0$.

Figure 18.- Driver to intermediate-chamber length ratio for configuration III.



(b) $(a_4/a_5)_{\bar{A}} = 10.0.$

Figure 18.- Continued.



(c) $(a_4/a_5)_{\bar{A}} = 20.0.$

Figure 18.- Concluded.

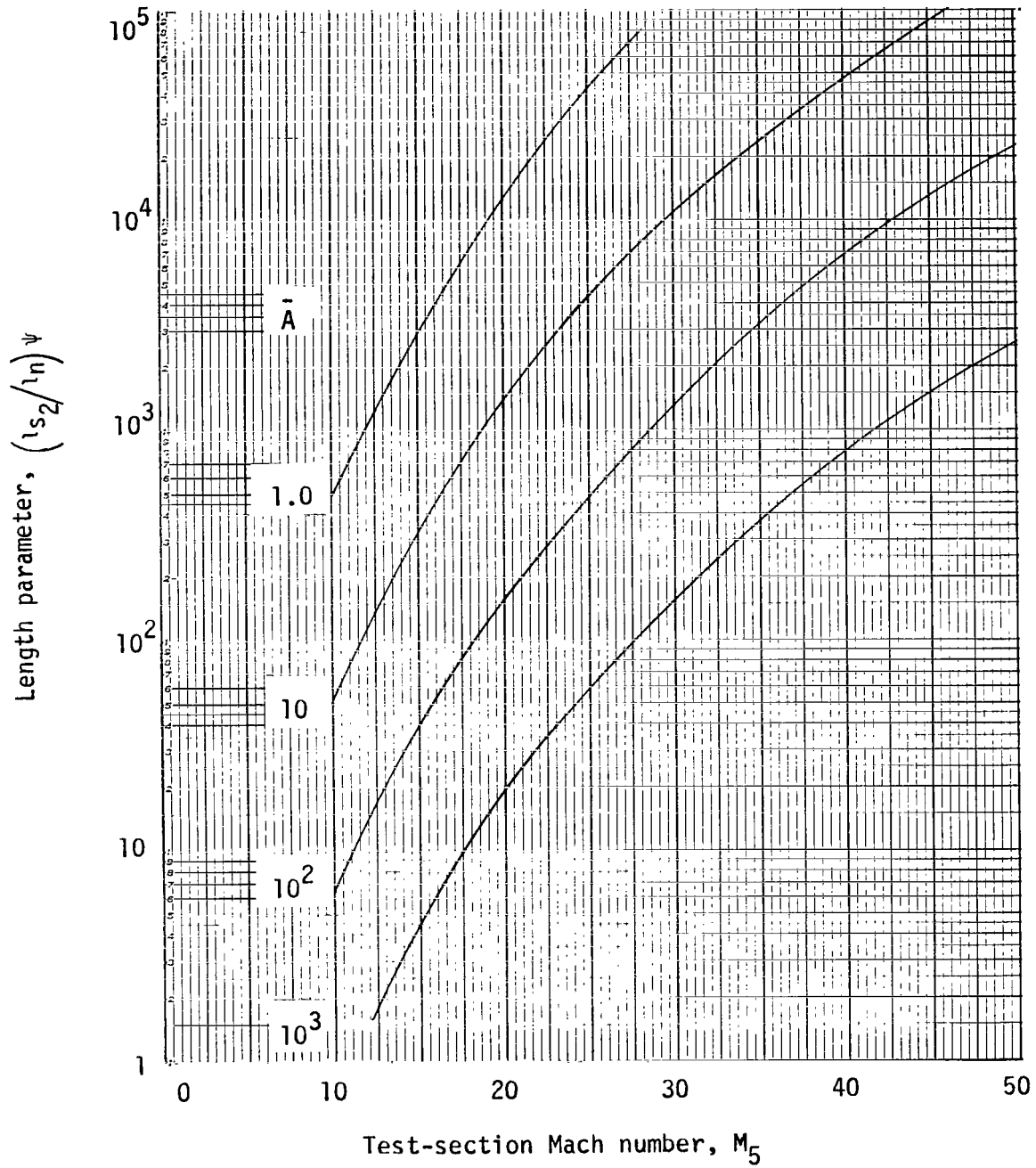


Figure 20.- Acceleration-chamber length parameter for configuration III.

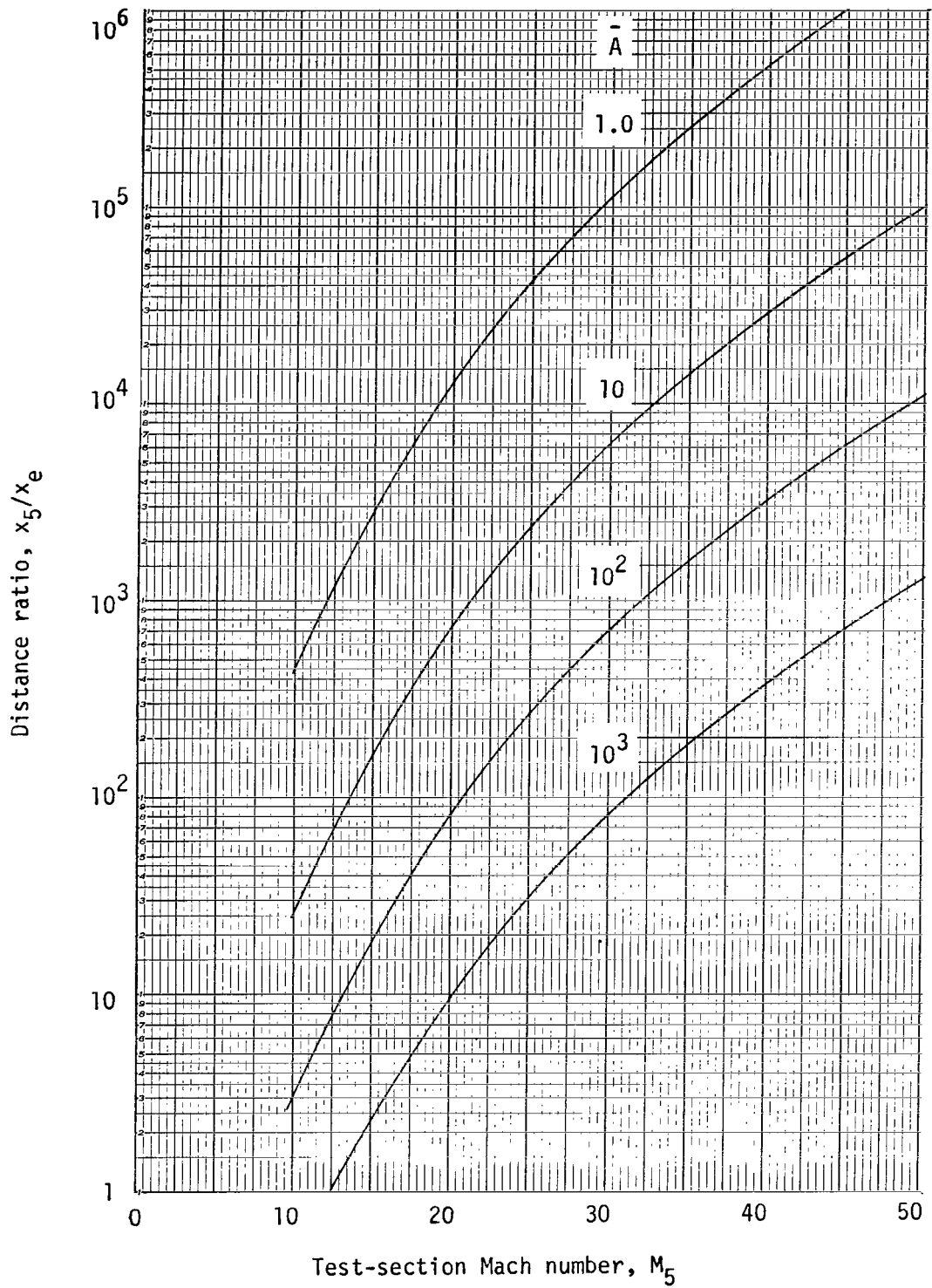


Figure 21.- Ratio of exit to entrance distances for flow particle in a $u - a$ expansion.

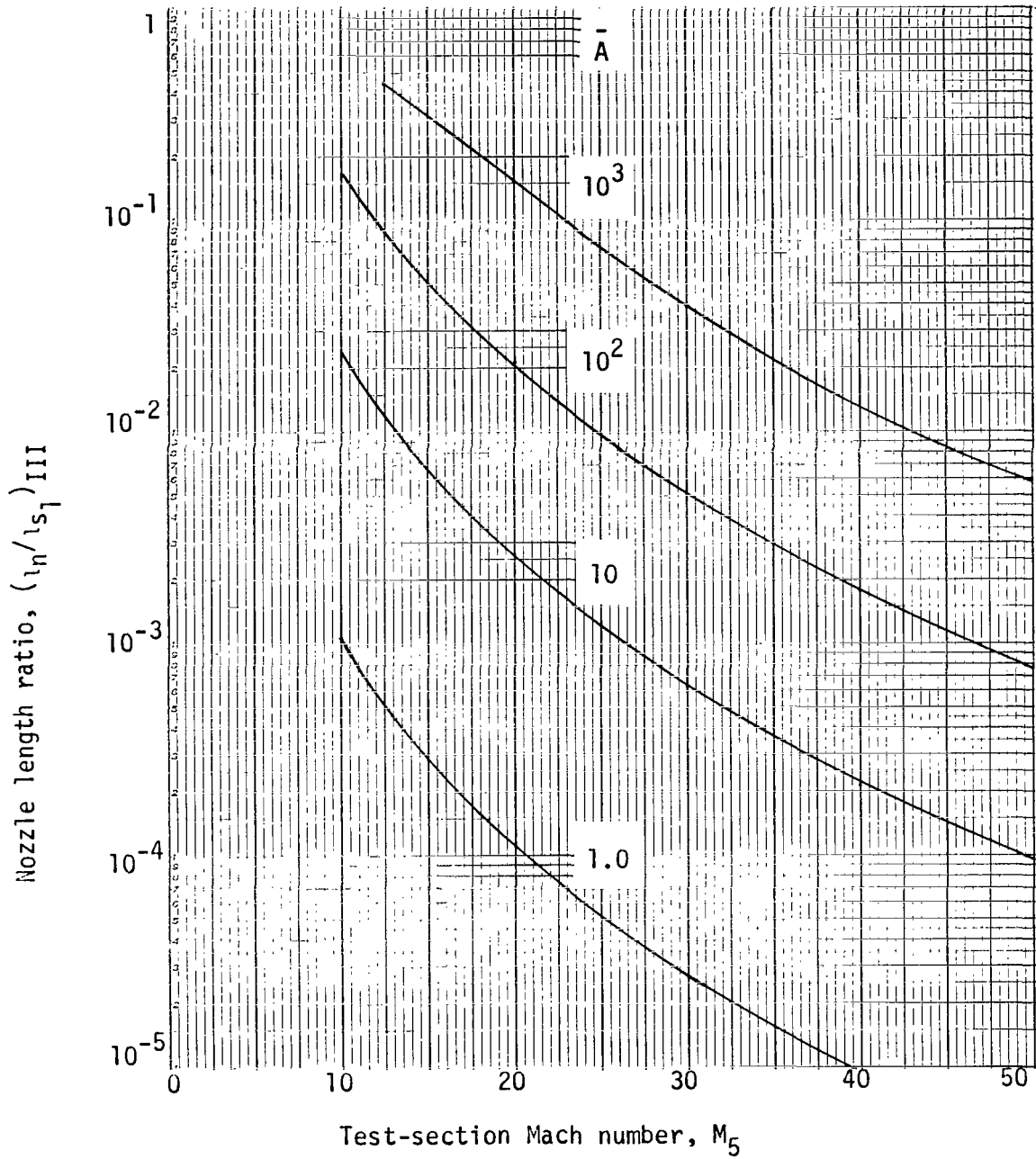


Figure 22.- Ratio of maximum nozzle length to acceleration-chamber length for configuration III.

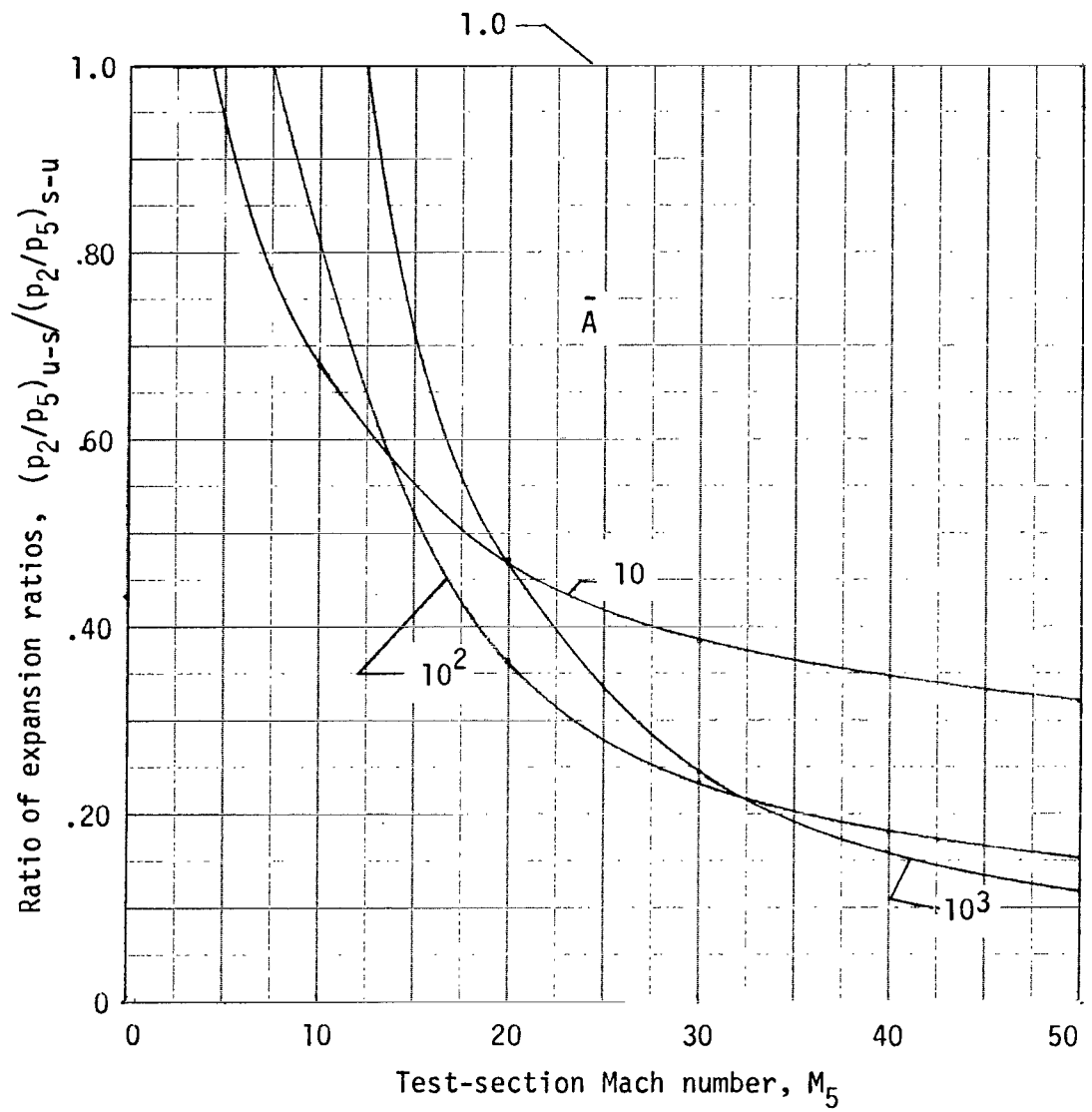


Figure 23.- Ratio of p_2/p_5 as given by unsteady followed by steady expansion to p_2/p_5 given by expansions in reverse order.

"The aeronautical and space activities of the United States shall be conducted so as to contribute . . . to the expansion of human knowledge of phenomena in the atmosphere and space. The Administration shall provide for the widest practicable and appropriate dissemination of information concerning its activities and the results thereof."

—NATIONAL AERONAUTICS AND SPACE ACT OF 1958

NASA SCIENTIFIC AND TECHNICAL PUBLICATIONS

TECHNICAL REPORTS: Scientific and technical information considered important, complete, and a lasting contribution to existing knowledge.

TECHNICAL NOTES: Information less broad in scope but nevertheless of importance as a contribution to existing knowledge.

TECHNICAL MEMORANDUMS: Information receiving limited distribution because of preliminary data, security classification, or other reasons.

CONTRACTOR REPORTS: Technical information generated in connection with a NASA contract or grant and released under NASA auspices.

TECHNICAL TRANSLATIONS: Information published in a foreign language considered to merit NASA distribution in English.

TECHNICAL REPRINTS: Information derived from NASA activities and initially published in the form of journal articles.

SPECIAL PUBLICATIONS: Information derived from or of value to NASA activities but not necessarily reporting the results of individual NASA-programmed scientific efforts. Publications include conference proceedings, monographs, data compilations, handbooks, sourcebooks, and special bibliographies.

Details on the availability of these publications may be obtained from:

SCIENTIFIC AND TECHNICAL INFORMATION DIVISION
NATIONAL AERONAUTICS AND SPACE ADMINISTRATION
Washington, D.C. 20546